A multi-proxy approach to decode the end-Cretaceous mass extinction

Jahnavi Punekar[1], Gerta Keller[1], Hassan M. Khozyem[2], Thierry Adatte[3], Eric Font[4], Jorge Spangenberg[3]

[1]*Geosciences, Princeton University, Princeton, NJ 08540, USA.*
[2]*Department of Geology, Faculty of Science, Aswan University, Aswan 81528, Egypt.*
[3]*Institute of Earth Sciences, University of Lausanne, 1015 Lausanne, Switzerland.*
[4]*IDL-FCUL, Instituto Dom Luís, Faculdade de Ciências, Universidade de Lisboa, Portugal, Campo Grande, 1749-016, Lisbon, Portugal.*

Corresponding Author:
Jahnavi Punekar
Phone: +1- 609-258-6482
Email: jpunekar@princton.edu

Abstract

Mass extinctions generally involve a complex array of interrelated causes and are best evaluated by a multi-proxy approach as applied here for the end-Cretaceous mass extinction. This study documents and compares the planktic foraminiferal records, carbonate dissolution effects, stable isotopes, and magnetic susceptibility in France (Bidart), Austria (Gamsbach) and Tunisia (Elles) in order to explore the environmental conditions during the uppermost Maastrichtian *Plummerita hantkeninoides* zone CF1 leading up to the mass extinction. Planktic foraminiferal assemblages at Bidart and Gamsbach appear to be more diverse than those at Elles, with unusually high abundance (20-30%) and diversity (~15 species) of globotruncanids in the two deep-water sections but lower abundance (<10%) and diversity (<10 species) at the middle shelf Elles section.

Oxygen isotopes in zone CF1 of Elles record rapid climate warming followed by cooling and a possible return to rapid warming prior to the mass extinction.

The onset of high stress conditions for planktic foraminifera is observed ~50-60 cm below the KTB at Bidart and Gamsbach, and ~4.5 m below the KTB at Elles due to much higher sediment accumulation rates. These intervals at Bidart and Gamsbach record low magnetic susceptibility and high planktic foraminiferal fragmentation index (FI) at Elles, Bidart and Gamsbach. An increased abundance of species with dissolution-resistant morphologies is also observed at Gamsbach. The correlative interval in India records significantly stronger carbonate dissolution effects in intertrappean sediments between the longest lava flows, ending with the mass extinction. Based on current evidence, this widespread dissolution event stratigraphically coincides with the climate cooling that follows the Late Maatrichtian global warming and may be linked to ocean acidification due to Deccan volcanism. The estimated 12,000–28,000 Gigatons (Gt) of CO_2 and 5200–13,600 Gt of SO_2 introduced into the atmosphere likely triggered the carbonate crisis in the oceans resulting in severe stress for marine calcifiers leading to the mass extinction.

1. INTRODUCTION

One of the best-known European Cretaceous-Tertiary boundary (KTB) sections, also known as Cretaceous-Paleogene (KPB or KPg) sections, is exposed at a beach near Bidart, in the Basque-Cantabrian basin of southwestern France (Figs. 1, 2B, Seyve, 1990; Haslett, 1994). At this locality about 8 m of uppermost Maastrichtian and ~4 m of basal Danian sediments are exposed, including the boundary clay, an Iridium (Ir) anomaly and negative $\delta^{13}C$ excursion that indicate a relatively complete KTB transition (Fig. 2A, C; Renard et al., 1982; Bonté et al., 1984; Apellaniz et al., 1997; Font et al., 2014). Nevertheless, the Bidart section remained in limbo for nearly two decades because of uncertain age control, particularly the reported absence of the latest Maastrichtian nannofossil *Micula prinsii* zone and absence of the planktic foraminiferal zones CF1 (*Plummerita hantkeninoides)* and CF2, which together are correlative with paleomagnetic chron C29r. This led to the assumption that the latest Maastrichtian is missing (Gallala et al., 2009). Subsequent paleomagnetic and microfossil studies revealed that the ~8 m of uppermost Maastrichtichtian sediments below the KTB were deposited during the *Micula prinsii* zone (Galbrun and Gardin, 2004) and the recent finding of *P. hantkeninoides* zone CF1 (Font et al., 2014) further confirms deposition in paleomagnetic chron C29r below the KTB boundary and hence a substantially complete KTB transition.

Restudy of the Bidart section is particularly important because of the potential connection between the high-stress interval spanning the last 50-cm of the Maastrichtian and Deccan volcanism in India (Font et al., 2011, 2014). As early as the 1990s, Apellaniz et al. (1997) reported a drop in carbonate content and increased planktic foraminiferal test

dissolution particularly in the KTB clay and the underlying 28-cm uppermost Maastrichtian sediments. This interval depleted in carbonate content is also featured by a loss of iron oxides (biogenic and detrital magnetite), interpreted to be the result of acidification linked to Deccan acid rains (Font et al., 2014; Font and Abrajevitch, 2014). The possible link between this dissolution interval and ocean acidification related to Deccan volcanism appears to be more than coincidental and warrants a fresh investigation of associated changes in planktic foraminiferal assemblages. Bidart therefore provides a unique opportunity to analyze this critical time interval in Earth history to understand the environmental changes in the northern mid-latitude Atlantic Ocean that may be related to the global effects of Deccan volcanism.

Preliminary faunal analysis of the Bidart section reveals a planktic foraminiferal assemblage remarkably different from those reported for El Kef (GSSP) and Elles, Tunisia, and other continental shelf locations (Abramovich et al., 2002; Font et al., 2014). To evaluate whether this is due to different depositional settings (open ocean bathyal depths for Bidart versus shelf depth for Tunisia), we chose a second bathyal section, Gamsbach, Austria, as a control site. Gamsbach is located in the Eastern Alps with a palaeogeographic setting and depositional history similar to Bidart (Figs. 1, 3B; Grachev et al., 2005). Gamsbach contains planktic foraminiferal assemblages similar to those at Bidart, including a pre-KTB dissolution interval that supports the choice of Gamsbach as a complementary site.

Although numerous studies have explored the KTB transition at Bidart and Gamsbach over the past three decades (see sections 1 and 2, supplementary material), the published microfossil records are generally not quantitative and at very low sample

resolution yielding little or no information for the critical pre-extinction interval. We present comprehensive biostratigraphic, assemblage and stable isotope, geochemical and mineralogical data that focus on the rapid climatic and biotic events of zone CF1, which globally record the crises that led up to the KTB mass extinction. The primary objective of this study is to test the hypothesis that Deccan volcanism may have caused global climate changes and ocean acidification that directly resulted in the KTB mass extinction recorded in planktic foraminifera.

We test this hypothesis based on: (1) High-resolution quantitative planktic foraminiferal species abundances through the uppermost Maastrichtian zones CF1-CF2 at Bidart and Gamsbach. (2) High-resolution biostratigraphic analysis with special emphasis on the presence/absence of index species (e.g., *Gansserina gansseri* and *Plummerita hantkeninoides*) to re-evaluate the conflicting published reports (reviewed below). (3) Evaluation of the palaeoclimatic and the paleoenvironmental conditions recorded in stable isotopes, geochemical proxies, and associated biotic events. (4) Evaluation of carbonate and iron oxide dissolution events based on the quality of foraminiferal test preservation (fragmentation index FI) and magnetic susceptibility, respectively. (5) Determination of the chronologic sequence of biotic, climatic and geochemical events through zone CF1 at Bidart and Gamsbach, as well as their regional and global oceanographic significance in the context of environmental perturbations related to Deccan volcanism. And (6) comparison with shelf sequences at Elles and El Kef, Tunisia, to assess the nature of environmental changes in shallow vs. deep-water environments.

2. BACKGROUND

2.1. Bidart and Gamsbach

Previous studies of the Bidart and Gamsbach sections report sedimentologic, geochemical, paleomagnetic and microfossil biostratigraphic data. A brief summary is given here (See supplementary material for details).

***Bidart*:** Planktic foraminifera and nannofossils record a rapid decline at the KTB at Bidart (Gorostidi and Lamolda, 1995; Thibault et al., 2004; Apellaniz et al., 1997; Gallala et al., 2009), whereas benthic foraminifera switch from infaunal to epifaunal dominance across the KTB (Alegret et al., 2004). An Iridium anomaly of 6.3±1.1 ppb, enrichment of Co, Cr, Ni, As, Sb, Se and depletion of rare earth elements (REE) are reported in the Bidart KTB red clay layer (Delacotte, 1982; Smit and Ten Kate, 1982; Bonté et al., 1984). Some studies report the presence of microtektites, microspherules and Ni-rich crystals in the KTB red layer in the Basque sections but provide no supporting data (Apellaniz et al., 1997; Arz and Arenillas, 1998; Arenillas et al., 2004).

***Gamsbach*:** Previous studies on Gamsbach show the KTB clay enriched in Ir (6 ppb), iron hydroxides, Co, Ni, Cr and siderophile elements and sporadic occurrence of pure Ni crystals, awaruite (Fe_3Ni), Ni-Fe, Ni-Fe-Mo and Ni-Fe-Co alloys, cosmic dust and spherules of varied geochemical affinities (Grachev et al., 2005, 2008; Pechersky et al., 2006; Egger et al., 2009). Micropaleontological and biostratigraphic studies are limited due to poor carbonate preservation throughout the KTB transition (Egger et al., 2004, Summesberger et al., 2009, Korchagin and Kollmann in Grachev, 2009). Summesberger et al. (2009) reported on the cephalopod, nannofossil and planktic foraminiferal biostratigraphy at Gamsbach but provided no quantitative documentation.

2.2. Deccan Volcanism

Deccan eruptions resulted in an estimated 1.5 million km^3 of lava flooding the Indian sub-continent (Raja Rao et al., 1999). Three main phases of eruptions are recognized: the initial phase-1 (~6% of the total volume) in the early late Maastrichtian recently dated by $^{40}Ar/^{39}Ar$ at 67.12±0.44 Ma at the chron C30n/C29r transition (Schoebel et al., 2014); the main phase-2 (~80% of the total lava pile) in chron C29r (Subbarao et al., 2000; Jay and Widdowson, 2008; Chenet et al., 2007, 2008; Schoene et al., 2014) culminating in the KTB mass extinction (Keller et al., 2011a, 2012); and the final phase-3 (~14% of the total volume) in the early Danian chron C29n. The environmental effects of the three Deccan phases are determined by the tempo and magnitude of eruptions and the amounts of SO_2, CO_2, Cl and other gases released into the atmosphere (Self et al., 2008). A global review of the planktic foraminiferal events contemporaneous with Deccan phase-2 and phase-3 can be found in Punekar et al. (2014a).

In the Krishna-Godavari Basin of SW India a rapid succession of four phase-2 lava mega-flows span C29r below the KTB and mark the CF1–CF2 and *Micula prinsii* (nannofossil) zones; intertrappean sediments reveal rapid extinctions (Keller et al., 2011a, 2012). The correlative interval in Meghalaya (NE India) is dominated (95%) by *Guembelitria* blooms, and high-stress is also marked by ocean acidification and strong carbonate dissolution (Gertsch et al., 2011). Schoene et al. (2015) show that the Phase-2 volcanism itself lasted ~500-kyr into the Danian. On a global basis paleoclimatic data from DSDP 525A (Li and Keller, 1998a), Tunisia, (Stüben et al., 2003) and Texas (Keller

et al., 2011b; Abramovich et al., 2011) show at least one and possibly multiple hyperthermal events during the CF1-CF2 global warming, which indicates complex and episodic climate fluctuations in the latest Maastrichtian correlative with Deccan phase-2 (Punekar et al., 2014a).

At Bidart and Gubbio Font et al. (2011, 2014) discovered akaganeite, an unusual Cl-bearing iron hydroxide preserved in a low magnetic susceptibility (MS) interval below the KTB. The origin of this low MS interval is explained by the loss of detrital and biogenic magnetites from reductive iron hydroxide dissolution due to acid rains and ocean acidification linked to Deccan Phase-2 (Font et al., 2014). They proposed a Deccan volcanic origin for akaganeite, formed by interaction of acid aerosols with the high atmosphere and potentially transported through the stratosphere at Bidart (Atlantic realm) and Gubbio, Italy (Tethys realm). If a volcanic origin for akaganeite is confirmed, this can provide a promising new geochemical benchmark for identifying Deccan environmental effects across the globe.

3. GEOLOGIC SETTING AND LITHOLOGY

3.1. Bidart, France

The Bidart KTB boundary section outcrops along the Erreteguia beach 2 km north of Bidart and can be accessed by the national highway R.N. 10 (W 1°35', N 43°26'; Fig. 2B). Sediments consist of hemipelagic to pelagic marls and limestones deposited at upper-middle bathyal depths in the Aturian Trough during the late Maastrichtian to Paleocene (Galbrun and Gardin, 2004; Alegret et al., 2004; Font et al., 2011). Deposition

183 occurred in a flysch zone and accumulated at 3-4 cm/ky, resulting in thick marl beds
184 (Seyve, 1984; Nelson et al., 1991; Clauser, 1994; Peybernes et al., 1997; Vonhof and
185 Smit, 1997). Tectonic disturbance (Pyrenean orogeny) and diapirism resulted in interbed
186 sliding, slickensides, and mass-flow deposits (Razin, 1989; Apellaniz et al., 1997).

187 About 8 m of uppermost Maastrichtian (C29r) pink to purple marlstones and
188 marls with occasional turbidites and cut by local faults are exposed below the KTB at
189 Bidart and can be traced throughout the Basque basin (Fig. 2A; Apellaniz et al., 1997). At
190 the base of the section analyzed is a 25-cm thick marlstone followed by ~2.5 m of marls
191 with common pelecypod shells and fragments. In the ~50-cm below the KTB carbonate
192 content decreases and macrofossils are absent, except at the top of this interval where
193 burrows are truncated by the overlying boundary clay.

194 The KTB is easily recognized by a 2 mm "rusty" layer at the base of an 8-15 cm
195 thick clay layer (Fig. 2B, C; Bonté et al., 1984; Apellaniz et al., 1997). The base of the
196 clayey interval is a grey to yellow silty clay overlain by red-brown siltstone and a thinly
197 laminated dark grey siltstone at the top. Carbonate content gradually increases in the
198 overlying basal Danian claystones, which are overlain by hemipelagic limestones marked
199 by alternating pink and white (occasionally glauconitic) biogenic limestones bioturbated
200 near the top of the section (Apellaniz et al., 1997; Font et al., 2011). At the top of the
201 outcrop is a mass-flow deposit with an erosive basal surface.

202

203 **3.2. Gamsbach, Austria**

204

205 The KTB boundary section is located in the Gamsbach valley of the Austrian
206 Alps (E 14°51'50; N 47°39'51; Figs. 3B). During the KTB transition the Gamsbach area

was located in the northwestern Tethys between paleolatitudes 20° to 30°N (Fig. 1; Haubold et al. 1999; Pueyo et al. 2007). The basin was formed after the early Cretaceous thrusting followed by transtension and subsidence due to subduction (Wagreich, 1993, 1995). Erosion at the front of the Austro-Alpine microplate resulted in deposition of sediments at middle bathyal depths (600-1000 m) during the late Maastrichtian and lower bathyal depth (>1000 m) in the early Danian (Egger et al., 2009).

Sediments consist of hemipelagic pelites interbedded with thin sandy turbidites (<15 cm) characteristic of the Nierental Formation of the Gosau group in the northern calcareous Alps (Wagreich and Krenmayr, 1993, 2005). The Maastrichtian is composed of medium gray marlstones and marly limestones. Truncated burrows mark the top of the Maastrichtian below the 2-cm thick clay layer that marks the KT boundary. This KT clay layer contains 0.2-0.4 cm thick yellowish clay at the base (Fig. 3A, C).

4. MATERIAL AND METHODS

Sampling at Bidart concentrated on the 3.5 m interval below the KTB with samples collected at 15-cm intervals for the bottom 3 m and 5-cm intervals for the top 50 -cm. At Gamsbach, 2 m of the uppermost Maastrichtian below the KTB were sampled at 5-6 cm intervals. In the laboratory, samples were crushed into small fragments and left overnight in 3% hydrogen peroxide solution to oxidize any organic carbon. The disaggregated sediment samples were then washed through >63 μm and >38 μm sieves (Keller et al., 1995). The washed residues were oven dried at 50°C. Quantitative faunal analysis was based on 63-150 μm and >150 μm size fractions. Each size fraction of every

sample was split with an Otto micro-splitter to obtain approximately 300 specimens of planktic foraminifera (for a statistical representation of the species population). These were picked, sorted and mounted on micro-slides and identified. The residual sample was searched for rare species and index species for biostratigraphy but not included in the quantitative dataset. Species identification is based on standard taxonomic concepts (e.g., Robaszynski et al., 1983-1984; Nederbragt, 1991; Olsson et al., 1999).

For the foraminifera fragmentation index, a microsplitter was used to obtain approximately 500-700 foraminifera and fragments from the >63 mm fraction such that at least 100 entire tests were counted. Three categories were identified based on the quality of preservation: entire (nearly) perfect tests (Plate 1, Plate 3: A-G), partially damaged (imperfect) tests (Plate 2: A-L; Plate 3: H-L, O, P) and fragments (Plate 2: M-T; Plate 3: M, N, Q-S). Specimens consisting of less than two-third of an entire test were counted as fragments (Berger et al., 1982). Planktic foraminifera fragmentation data was obtained for Bidart, Gamsbach and Elles sections. Benthic foraminifera fragmentation data was also obtained for Bidart to account for mechanical breakage due to post-depositional transport and sample processing techniques.

Stable carbon and oxygen isotope analyses were performed on whole-rock samples from Gamsbach for this study. These analyses were conducted using a Thermo Fisher GasBench II preparation device interface with a Thermo Fisher Delta Plus XL continuous flow isotope ratio mass spectrometer at the Institute of Earth Surface Dynamics (IDYST) of the University of Lausanne, Switzerland. The stable carbon and oxygen isotope ratios are reported in delta (δ) notation as permil (‰) deviation relative to the Vienna Pee Dee belemnite (VPDB). Whole rock and clay mineral data were acquired

253 from XRD analyses using SCINTAG XRD 2000 Diffractometer at the Geological
254 Institute of the University of Lausanne, Switzerland. The procedure for sample
255 processing was based on Adatte et al. (1996).

256 Mass specific magnetic susceptibility (MS) was measured at the Institute Dom
257 Luís (IDL), at the University of Lisbon, Portugal with a MFK-1 (AGICO). Rock
258 fragments were crushed by using an agate mortar and filled within typical cubic plastic
259 boxes of 8 cm^3 in volume. MS values are reported relative to mass (m^3/kg).

260

261 **5. BIOSTRATIGRAPHY: HOW COMPLETE IS THE KTB TRANSITION?**

262

263 To evaluate the stratigraphic completeness of the KTB transition we apply the
264 high-resolution planktic foraminiferal zonal scheme by Li and Keller (1998a,b) and
265 Keller et al. (1995, 2002a) (Fig. 4). The KTB is placed at 65.5 Ma (Gradstein et al.,
266 2004). However, the precise age of this boundary event is in flux with more recent
267 geochronologic dating suggesting an age closer to 66.0 Ma (Renne et al., 2013) and
268 additional dating still in progress. Based on cyclostratigraphy the duration for
269 paleomagnetic chron C29r is estimated at 750 ky with the base of C29r at 66.25 Ma
270 (Gradstein et al., 2004; Schoene et al., 2014; Thibault et al., this vol.).

271 ***Uppermost Maastrichtian Zone CF1:*** This zone is defined by the total range of
272 the index species *P. hantkeninoides.* Previous studies concluded that *P. hantkeninoides* is
273 absent at Bidart (Arz and Molina, 2002; Gallala et al., 2009; Galalla, 2013). However, we
274 observed this species in the 5 m below the KTB (see also Font et al., 2014) and 1.75 m
275 below the KTB at Gamsbach (Supplementary material Section 3). This indicates that in

both localities the uppermost Maastrichtian zone CF1 is present. Zones CF1 and CF2 are equivalent to the upper part of the nannofossil *M. prinsii* zone, which spans the top 8 m of the Bidart section (Galbrun and Gardin, 2004) and corresponds to C29r below the KTB. The sediment accumulation rate for this interval is 3.2 cm/ky (800 cm/250ky) and 3.1 cm/ky for zone CF1. Previous studies estimated a sedimentation rate of 4 cm/ky for the Maastrichtian distal sea fan at Bidart (Seyve 1990; Nelson et al., 1991; Vonhof and Smit, 1997) and 2.5 cm/ky for the nearby Sopelana section (Mary et al., 1991). This study suggests that the zone CF1 interval is substantially complete, although truncated burrows at the top of CF1 just below the KT boundary clay suggest some erosion. Compared with the middle bathyal environment at Bidart, the middle shelf depositional environment at Elles, Tunisia, reveals a much higher sediment accumulation rate of 8.6 cm/ky for C29r below the KTB. Based on this section, the duration of zone CF1 is estimated at ~160 ky based on the KTB at 65.5 Ma (Gradstein et al., 2004). Considering the KTB at 66 Ma and the C30n/C29r transition at ~66.288 Ma, zone CF1 at Elles is ~130 ky long (Renne et al., 2013; Schoene et al., 2014)

At Gamsbach, *P. hantkeninoides* was identified in the top ~1.75 m of the Maastrichtian for the first time in this study (Fig. 6B, Plate 1: M). Truncated burrows mark the top of zone CF1 below the boundary clay similar to Bidart. Based on these observations we conclude that the upper part of zone CF1 to the KTB mass extinction at Gamsbach is similar to Bidart and substantially complete. The abrupt negative $\delta^{13}C$ shift in bulk rock at the KTB and the presence of an erosional surface truncating burrows at both Gamsbach and Bidart suggests some erosion. Biostratigraphy indicates that erosion was primarily of basal Danian sediments.

299 ***KT boundary clay Zone P0:*** The KTB consists of a "boundary clay" zone P0
300 overlying the Maastrichtian mass extinction horizon. The boundary is easily identified on
301 the basis of five globally verified criteria: (1) mass extinction of Cretaceous planktic
302 foraminifera, (2) appearance of the first five Danian species within a few cm of the
303 boundary clay, (3) KTB clay and red layer, (4) an Ir anomaly and (5) the $\delta^{13}C$ negative
304 shift (Keller et al., 1995; 2011b). The KTB is also characterized by an abrupt increase in
305 magnetic susceptibility (Font et al., 2011; this study). At Bidart and Gamsbach, the KTB
306 clay is very thin (~5 cm and ~3 cm respectively) and overlies an erosion surface with
307 truncated burrows. The zone P0 clay, which is defined by the interval between the mass
308 extinction horizon and first appearance of *Parvularugoglobigerina eugubina*, is absent as
309 this species directly overlies the mass extinction horizon. Ir anomalies of 6.3 ppb and
310 ~6.0 ppb at Bidart and Gamsbach, respectively (Bonté et al., 1984; Vonhof and Smit,
311 1997; Egger et al., 2009) are concentrated in the thin clay that represents redox conditions
312 above the erosion surface. Similarly, the $\delta^{13}C$ negative shift of 2.0 to 2.3‰ is abrupt
313 across the erosion surface in both sections (Rocchia et al., 1987; Font et al., 2014). In
314 comparison, at the stratotype El Kef and expanded Elles sections in Tunisia, the P0 clay
315 is 50 to 75 cm thick with an Ir anomaly of 18 ppb at the base and a 4‰ negative carbon
316 isotope excursion (Rocchia et al., 1996; Stuben et al., 2003). The relative time
317 represented by the condensed P0 intervals and hiatuses at Bidart and Gamsbach can be
318 estimated based on the zone P1a planktic foraminiferal assemblages.
319 ***Zone P1a hiatuses:*** This zone is defined by the total range of *P. eugubina* and/or
320 *P. longiapertura* and can be subdivided into subzones P1a(1) and P1a(2) based on the FO
321 of *Parasubbotina pseudobulloides* and/or *Subbotina triloculinoides* (Fig. 4). At the time

322 of the P0/P1a(1) boundary only about five early Danian species had evolved and all were
323 rare as the assemblages were dominated by the Cretaceous survivor and disaster
324 opportunists *Guembelitria* species (review in Keller and Pardo, 2004).

325 At Bidart, zone P1a(1) directly overlies the mass extinction with common
326 *Parvularugoglobigerina extensa*, *P. eugubina* and *P. longiapertura*, an assemblage that is
327 known to first appear well into zone P1a(1) about 100 kyr after the KTB mass extinction
328 (Fig. 5A). This indicates that the early evolution of Danian species in P0 and lower part
329 of P1a(1) is missing due to erosion or non-deposition (Fig. 4). About 30-cm above this
330 hiatus subzone P1a(1) ends with another sudden faunal assemblage change marked by
331 dramatically decreased *Guembelitria*, *P. eugubina* and *P. longiapertura*, a sudden
332 appearance of abundant *Chiloguembelina morsei* and the FO of *S. triloculinoides* (Fig.
333 5A). This assemblage is indicative of subzone P1a(2) and marks another short hiatus
334 between subzones P1a(1) and P1a(2) (Fig. 4). Hiatuses at the KTB and lower Danian
335 (resulting from condensed sedimentation and/or deep-sea currents) have been
336 documented worldwide in various studies (reviews in MacLeod and Keller, 1991; Keller
337 et al., 2003, 2013).

338 At Gamsbach an early Danian hiatus is also present as evident by the diverse (12
339 species) early Danian assemblage including *P. pseudobulloides*, the index species for
340 subzone P1a(2) directly overlying the mass extinction horizon (Fig. 6A). This indicates
341 erosion of P0, P1a(1) and at least part of P1a(2) (Fig. 4). Another abrupt faunal change
342 and hiatus occurs at the P1a(2)/P1b boundary about 30-cm above the KTB marked by the
343 extinction of *P. eugubina* and *P. longiapertura* (index for top P1a(2)) and terminal
344 abundance decrease in *Globigerina edita*. Above this hiatus abundant *C. morsei* and

345 common *P. pseudobulloides* followed by abundant *Guembelitria* spp. indicates zone P1b
346 (Figs. 4, 6A).
347
348 **6. STABLE ISOTPES AND FAUAL TURNOVER**
349
350 **6.1. Stable isotopes**
351 Whole-rock stable carbon and oxygen isotope data for Gamsbach (Austria) were
352 obtained for this study (supplementary materials Table 7). Planktic, benthic and bulk
353 stable isotope data for Elles (Tunisia) and whole-rock isotope data for Bidart (France)
354 have already been documented (Stüben et al., 2003; Thibault et al., this vol.; Font et al.,
355 2014). Visual inspection of preservation and degree of recrystallization of individual
356 foraminifera tests indicated that the Gamsbach isotope data were likely to be the most
357 compromised.
358 At Elles, the overall low $\delta^{18}O$ values (-7.0 to -4.0‰) for planktic as well as
359 benthic (-4.5 to -2.0‰) foraminifera indicate diagenetic effects but long term trends may
360 still be preserved (Stüben et al., 2003; supplementary materials Table 5). At Bidart, the
361 whole-rock $\delta^{13}C$ values range between -1.7 and 1.8‰ and bulk $\delta^{18}O$ values range
362 between -3.2 and -0.3‰. Plotting $\delta^{13}C$ vs. $\delta^{18}O$ values yields a correlation coefficient
363 R^2=0.53, suggesting that diagenetic alteration of the primary signal may not be ruled out
364 (supplementary materials Table 6). A low $\delta^{13}C$ event is recognized between 3.5 m and
365 0.75 m below the KTB. A similar event is also observed in the planktic $\delta^{13}C$ values at
366 Elles between 1.75 m and 6.6 m below the KTB boundary indicating that this signal may
367 be real (Fig. 7). A long term increasing trend through zone CF1 is observed in $\delta^{18}O$

368 profiles of Bidart, Gamsbach and Elles, although the values at Gamsbach and Elles
369 record frequent fluctuations (Fig. 8). The whole-rock $\delta^{13}C$ values for Gamsbach range
370 between 1.41 to 2.42‰ and the bulk $\delta^{18}O$ range between -2.6 and -1.1‰. The $\delta^{13}C$ vs.
371 $\delta^{18}O$ correlation coefficient is lower than that for Bidart (R^2=0.27) but the poorly
372 preserved fragmented and recrystallized tests suggest considerable overprint on the
373 primary isotopic composition. The low $\delta^{13}C$ event of Bidart and Elles is not preserved at
374 Gamsbach.
375
376 **6.2. Faunal Turnover**
377 ***Bidart (France)***
378 Maastrichtian planktic foraminifera at Bidart are recrystallized but relatively well
379 preserved and identification is fairly easy. About 51 species were identified in the 63-150
380 μm size fraction and 23 species in the >150 μm size fraction (Fig. 5A). The species
381 richness in the 63-150 μm fraction gradually drops from 30 to 20 through the analyzed
382 interval of zone CF1. A rapid decline from ~20 species to 3 species is seen 3-cm below
383 the KTB. A brief increase to 13 species occurs 2-cm above the boundary clay is observed
384 in the small and large size fractions and is likely due to erosion and redeposition (Fig.
385 5A). In the >150 μm fraction, diversity remains nearly constant through CF1 but declines
386 from ~50 species to 11 species at 3-cm below the KTB.
387 All typical late Maastrichtian globotruncanids, rugoglobigerinids, heterohelicids
388 and pseudoguembelinids are represented, although the biserial heterohelicids and
389 pseudoguembelinids dominate the assemblages in the 63-150 um (Fig. 5B). In addition to
390 common cosmopolitan species, biserial species *Hartella harti* and *Spiroplecta americana*

391 Ehrenberg are also frequent in the assemblage (Plate 1: K, J); these species were first
392 described by Georgescu and Abramovich (2009) from upper Maastrichtian sediments of
393 the Atlantic Ocean. At Bidart *H. harti* and *Heterohelix navarroensis* are the most
394 abundant and together constitute 40-60% of the assemblage throughout CF1 (Figs. 5B, 7;
395 Plate 1: K, L). *Guembelitria* sp. is present in the 63-150 μm size fraction but not in the
396 abundance observed in shallow marine KTB transitions (e.g. Egypt, Sinai, Tunisia
397 (Seldja); Keller and Benjamini, 1991; Keller et al., 1997; Keller, 1998b; 2002b; Punekar
398 et al., 2014b; Plate 1: I). The newly evolved Danian assemblage in zone P1a(1) is
399 dominated by *Guembelitria sp*. and *Parvularugoglobigerina sp*. (30-40%, Fig. 5A). The
400 P1a(2) assemblage is dominated by *Chiloguembelina midwayensis.* (See supplementary
401 material Fig. S1 for planktic foraminifera in the >150 μm size fraction at Bidart)

402 ***Gamsbach (Austria)***

403 A planktic foraminiferal study by Korchagin in Grachev et al. (2005) identified
404 only 25 Maastrichtian species and placed this assemblage in the *Abathomphalus*
405 *mayaroensis* zone, which spans most of the late Maastrichtian (68.72 – 65.5 Ma). The
406 preservation of Maastrichtian planktic foraminifera in the 63-150 μm fraction at
407 Gamsbach is very poor. Recrystallization and the difficulty of freeing specimens from
408 surrounding sediments result in specimens with a highly fragmented and abraded
409 appearance and no reliable quantitative data can be obtained for the Maastrichtian
410 (supplementary material Fig. S2). In the >150 μm fraction preservation is better and
411 therefore was analyzed quantitatively (Fig. 6B). A total of 46 species were identified in
412 the >63 μm size fraction which is likely an underestimate of the total assemblage due to
413 poor preservation. Most species are consistently present in the lower 1.25 m of the

414 section. But in the uppermost 0.5 m, species are more sporadic and species richness drops
415 from 46 to 21-30 species. In the >150 μm fraction, species richness ranges between 30-40
416 species and drops from ~25 to 8 species at the KTB (Fig. 6A).

417 All common Maastrichtian groups such as the globotruncanids, rugoglobigerinids,
418 heterohelicids and pseudoguembelinids are present in the assemblage. *Pseudotextularia*
419 *elegans, Pseudotextularia nuttali, Pseudoguembelina hariaensis, Heterohelix globulosa*
420 and *Planoglobulina brazoensis* dominate the >150 μm fraction (Fig. 6B). *Guembelitria*
421 sp. is almost absent in the 63-150 μm fraction. In contrast to Bidart, *H. harti* and *S.*
422 *americana* are not present in the assemblage (Fig. 8C). In the Danian, the diversity in
423 zone P1a(2) is about 10 species which increases to ~20 species in zone P1c. The P1a(2)
424 assemblage overlying the KTB is dominated by *G. cretacea, P. eugubina, P.*
425 *longiapertura, Globigerina edita, Globanomalina archaeocompressa* and *Praemurica*
426 *taurica* (Fig. 6A).

427

428 **6.3. Depth-ranked species**

429 Planktic foraminifera species have been classified into surface dwelling
430 opportunistic species *Guembelitria*, surface-subsurface mixed layer, intermediate or
431 thermocline and deep-water dwellers based on stable oxygen and carbon isotope ranking
432 of well-preserved specimens (Abramovich et al., 2003, 2010). The diversity and
433 abundance changes for each depth group can indicate climatic and environmental effects
434 at different depths of the water column. Figure 9 shows the diversity and abundance of
435 the four groups in small (63-150 μm) and larger (>150 μm) size fractions analyzed
436 through zone CF1 at Bidart and Gamsbach and compared with Elles, Tunisia

437 (Supplementary material Section 5, Table 1 show the depth-ranked grouping of species
438 used for this study).

439 At Bidart, the small sized opportunistic *Guembelitria* (63-150 μm fraction) are
440 rare in the lower part of the section and slightly increase in the upper ~1.5 m below the
441 KTB (Fig. 9B). This group is not as rare in Elles but the relative abundance is <10% (Fig.
442 9A). The subsurface mixed layer dwellers (Table 1) constitute 80-90% of the CF1
443 assemblage at both Bidart and Elles. In the small size fraction, this group at Bidart with
444 30-40 species is almost twice as diverse as at Elles, (10-20 species). In the >150 μm
445 fraction, the relative abundance of mixed layer dwellers constitute 60-80% at Bidart and
446 ~80% at Elles (Fig. 9A, B). Their diversity fluctuates through CF1 and shows a gradual
447 decrease from ~20 to 14 species followed by a rapid decline ~3 cm below the KTB. The
448 thermocline dwelling globotruncanids are rare in the small size fraction at both Bidart
449 and Elles with relative abundance <5%. Two peaks of increased abundance and diversity
450 are noted in the upper 30-cm of late Maastrichtian at Bidart and in the last meter at Elles.
451 In the >150 μm fraction, thermocline dwellers are more abundant (20-30%) at Bidart
452 compared to the same group in Elles (<10%). The sub-thermocline deep-water dwellers
453 in both size fractions at Bidart and Elles show consistently low abundances (<5%) and
454 diversity (<3 species) throughout zone CF1 (Fig. 9A, B).

455 At Gamsbach the mixed dwellers dominate in the larger size fraction, with ~70%
456 relative abundance, followed by the thermocline dwellers with 25-30% abundance. The
457 high abundance of thermocline dwelling globotruncanids in Gamsbach is more
458 comparable to the assemblage at Bidart than that at Elles (Fig. 9C). The deep dwellers are
459 represented by 1-3 species and account for <10% throughout CF1.

460 The faunal assemblage differences between Elles vs. Bidart and Gamsbach appear
461 to be related to deposition in a relatively shallow continental shelf vs. deep middle
462 bathyal environments. This is indicated by the similarity in the faunal compositions
463 between Bidart, Gamsbach and the middle bathyal DSDP Site 525A, but dissimilarity
464 with Elles. For example (1) there is significantly higher relative abundance of *P.*
465 *hariaensis* at Bidart (20-25%), Gamsbach (10-20%) and Site 525A (10-20%), compared
466 with Elles (<5%) Abramovich and Keller, 2002; 2003); (2) *Heterohelix globulosa* is less
467 abundant in the >150 μm fraction at Bidart (15-20%), Gamsbach (<10% with acme of
468 20%) than at Elles (40-50%); (3) *Planoglobulina brazoensis* is more abundant (5-10%) in
469 all three deeper sections, but rare at Elles; and (4) *Globotruncana arca* is more abundant
470 at Bidart (10%), Gamsbach (10-20%) and Site 525A (20-30%) than at Elles (<5%).
471
472
473 **7. DISSOLUTION-BASED PROXIES FOR OCEAN ACIDIFICATION**
474
475 **7.1 Magnetic Susceptibility (MS)**
476 Magnetic susceptibility (MS) of marine deposits depends essentially on their
477 mineralogical composition, and includes contributions (in proportion to their abundance)
478 from all - diamagnetic (e.g., calcite), paramagnetic (e.g., clay) and ferromagnetic (ex:
479 magnetite) - minerals present in the sediment. Since the pristine signal of magnetic
480 susceptibility in marine sediment reflects the balance between detrital input (high MS)
481 and carbonate productivity (low MS), it represents a robust paleoenvironmental indicator.
482 The rock magnetic properties for Elles are published in Stüben et al. (2003) and for
483 Bidart in Font et al. (2011, 2014) and Font and Abrajevitch (2014).

Mass specific magnetic susceptibility values of the Maastrichtian marls from Elles are in the range of 10^{-7} to 10^{-6} m^3/kg, and comparable to other marine sediments worldwide (Ellwood et al., 2008). The overall MS profile for zones CF3-CF1 shows a positive correlation with percent phyllosilicates and an inverse correlation with carbonate content, indicating a strong relationship between MS, climate (precipitation and runoff) and/or sea-level rise. The KTB is featured by an abrupt shift in MS values, probably resulting from an abrupt change in lithofacies (i.e. the clay layer). The Elles section does not show the typical low MS interval below the KT boundary as in Bidart (Fig. 10A). At Bidart the average MS value is $1.85x10^{-7}$ m^3/kg for the lower part of zone CF1 and ~$0.84x10^{-7}$ m^3/kg for the final ~60 cm that forms the benchmark interval. The characteristic abrupt increase in MS values (to $4.62x10^{-7}$ m^3/kg, likely due to or a very rapid change in sedimentation) marks the KTB hiatus at Bidart (Fig. 10B). For the Gambsach section, the mass specific magnetic susceptibility of 49 samples excluding turbiditic levels was measured (Fig. 10C). Maastrichtian MS values range between 10^{-8} to 10^{-7} m^3/kg. The average MS value for the lower part of zone CF1 is $6.7x10^{-8}m^3$/kg. About ~60 cm below the KTB, MS values reach a minimum of 4.5 $x10^{-8}m^3$/kg (average of $5.1x10^{-8}m^3$/kg). These low MS values persist over an interval of 36-cm. Across the KTB MS values show the typical increase culminating at $2.3x10^{-7}m^3$/kg, similar to Bidart and other KTB sections (e.g., Gubbio, Oman: Ellwood et al., 2003; Atlantic ODP 1259: Erbacher et al., 2004; North Atlantic ODP 1049A: Moore et al., 1998).

7.2. Percent calcium carbonate

Whole-rock percent $CaCO_3$ content of marine sediments is the net result of the local paleaoclimate, calcareous nannoplankton and calcareous dinoflagellate palaeoproductivity, planktic foraminiferal abundance, water column pH/dissolution, pore-water dissolution/re-crystallization and detrital influx. For localities with greater terrigenous influx the ratio of Ca/detritus is a better estimate of biogenic $CaCO_3$ as it accounts for the detrital contribution. At Elles, the calcite/detritus ratio is low (0.5) near the base of zone CF1 (8-10 m below the KTB, Fig. 10A). In this interval, the phyllosilicate content is relatively high (25-35%) with an increasing trend. The Ca/detritus ratio fluctuates but increases to 0.75-1.00 about 5-8 m below the KTB along with an increase in MS values. The Ca/detritus ratio is higher in the top 4 m of zone CF1, albeit with three sharp decreases.

The percent $CaCO_3$ at Bidart gradually decreases from 55% at the base of zone CF1 to about 40% 2 m below the KTB. An increase to 50% is observed 1.5 m below KTB followed by values between 40-50% up to the low MS interval where values sharply increase to 60% about 0.25 m below the KTB (Fig. 10B). At Gamsbach, $CaCO_3$ ranges between 40-50% and records several abrupt decreases in zone CF1 correlative with abrupt changes in percent quartz and MS values (Fig. 10C). In the 1m below the KTB $CaCO_3$ varies between 55-80% with the largest drop ~20 cm below the KTB correlative with increased phyllosilicates and MS values. A drop in $CaCO_3$ to nearly zero percent is indicated in the KTB clay in all three sections.

7.3 Fragmentation index

Tests of planktic as well as benthic foraminifera may undergo fragmentation due to a multitude of taphonomic processes. Acidic ambient waters react with planktic foraminiferal test carbonate, which leads to test dissolution and enhanced fragmentation. The number of fragments have been used as a quantitative estimate of low pH in foraminiferal assemblages (Thunell, 1976; Berger et al., 1982). The fragmentation index may be calculated based on the following equation (Williams et al., 1985; Malmgren, 1987):

$$\text{Fragment \%} = (\text{Fragments}/8)/[(\text{Fragments}/8) + \text{whole tests}]$$

Based on the assumption that each (non-crystallized) test breaks into an average of 8 fragments, the equation requires the total number of counted fragments to be divided by 8 to estimate the original number of whole tests. This is because the number of fragmented tests is a better approximation of dissolution effects than the total number of fragments counted (Le and Shackleton, 1992). As most of the planktic foraminifera at Bidart, Elles and Gamsbach are recrystallized and/or infilled with secondary calcite, they are relatively more resistant to fragmentation than pristine tests. We adjust for recrystallization by reducing the number of fragments per test to 6 instead of 8 to avoid underestimation of fragmented tests. Similarly, we consider 2 fragments per test for benthic foraminifera for Bidart as they are far more resistant to fragmentation.

The stacked area graphs of Fig. 10 show fragmentation indices for Elles, Bidart and Gamsbach. At Elles, fragmented tests increase from 23% to 46% at the beginning of the low MS interval and increased fragmentation and imperfect tests are observed in the top 4 m below the KTB (Fig. 10A). At Bidart, the percentage of imperfect tests for the lower part of CF1 is considerably higher than at Elles and that of fragmented tests is

554 lower (Fig. 10 A-B). In the uppermost ~60 cm of zone CF1, the low-MS interval is
555 accompanied by a significant (p<0.0001) increase in the combined abundance of
556 imperfect and fragmented from ~25% to 70% (~0.3 m below KTB, Fig. 10B). A drop in
557 this percentage ~2.5 m below the KTB boundary is followed by a rapid increase to 90%.
558 It must be noted that the fragmented tests (not the imperfect tests) dominate at the KTB
559 boundary hiatus. The fragmentation index at Gamsbach also shows an abrupt increase in
560 the combined abundance of fragmented and imperfect tests from 40% to ~90% at the
561 onset of the low MS interval ~50 cm below the KTB boundary. Within this interval,
562 fragmentation continues to be high (~90%) up to the KTB boundary (Fig. 10C). A brief
563 episode of decreased fragmentation is observed ~20 cm below the KTB boundary similar
564 to the event recorded at Bidart (supplementary material Tables 2-4). Figure 11 compares
565 the fragmentation indices of planktic and calcareous benthic foraminifera at Bidart. The
566 proportion of fragments of benthic foraminifera remains 2-3 % for most of the analyzed
567 CF1 interval (Plate 3: M, N, Q-S). This is consistent with the general robustness of
568 benthic morphologies and likely indicates a limited/uniform influence of sample
569 processing techniques and post-depositional breakage on the assemblage. However, an
570 increase in the fragments to ~5% concurrent with the Deccan benchmark event may
571 imply enhanced post-depositional bottom water transport during the climate-cooling
572 event (Figs. 10, 11). The imperfect benthic tests of CF1 largely show mechanical damage
573 unlike the planktic counterparts that show chemically leached surfaces and holes (Plate 2:
574 A-L). However, at the KTB and the lowermost Danian, sediments contain benthic
575 foraminifera that show intense leaching as well as mechanical damage strongly indicating
576 a dominance of post-depositional dissolution and bottom water transport affecting the

577 assemblage. The planktic FI is not useful to isolate water column dissolution effects in
578 these samples (Fig 11).
579
580 **7.4 Preferential preservation of robust morphologies**
581 Dissolution preferentially decreases the relative abundance of thin-walled test
582 morphologies and therefore increases the relative abundance of robust dissolution-
583 resistant tests (e.g. *Globotruncana, Globotruncanita, Pseudotextularia* and *P.*
584 *brazoensis*), which may explain the increased calcite at this interval. This bias is evident
585 just below the KTB mass extinction in all three profiles analyzed. In the middle shelf
586 environment of Elles, globotruncanids and pseudotextularids are rare in zone CF1 (~1%),
587 increase to 2% in the low-MS interval and peaks at 10% and 6% in the 1 m preceding the
588 mass extinction (Fig. 10A). In the middle bathyal sections of Bidart and Gamsach, the
589 abundance of globotruncanids average 20-30% throughout zone CF1. At Bidart
590 globotruncanids abruptly reach 70% correlative with increased fragmentation and
591 decreased percent $CaCO_3$ beginning about 30-cm below the KTB (Fig. 10B). At
592 Gamsbach, globotruncanids and another robust species (*Planoglobulina brazoensis* show
593 anomalously high abundance throughout zone CF1 with peak abundance of *P. brazoensis*
594 correlative with the high fragmentation index ~15 cm below the KTB (Fig. 10C).
595
596 **8. DISCUSSION**
597
598 **8.1 Paleoclimate**

599 Whole-rock stable oxygen and carbon isotopes approximate mixed layer (mostly
600 calcareous nannoplankton) values in the deep-water sediments at Bidart and Gamsbach.
601 Diagenesis and recrystallization of tests may have overprinted $\delta^{18}O$ signals but their
602 effects on the $\delta^{13}C$ trend are limited. This claim is supported by the low correlation
603 coefficients of $\delta^{13}C$ vs. $\delta^{18}O$ (Stüben et al., 2003; R^2=0.53 for Bidart and R^2=0.27 for
604 Gamsbach) and the low correlation coefficient of $\delta^{13}C$ v/s %$CaCO_3$ (R^2=0.40 for Bidart
605 and R^2=0.39 for Gamsbach).
606 The lower ~3 m of zone CF1 at Bidart and lower ~1.2 m of Gamsbach record
607 faunal responses comparable with those observed in the upper part of the late
608 Maastrichtian global warming at Elles and DSDP Site 525A. Globally, this warm event
609 began in zone CF2 as a likely consequence of the onset of the main phase-2 of Deccan
610 volcanism (Punekar et al., 2014a). This is consistent with the more negative $\delta^{18}O$ values
611 for these intervals indicating higher temperatures (-2‰ for Bidart and -1.5 to -2‰ for
612 Gamsbach, Fig. 8). At Bidart, the late Maastrichtian warm event is associated with
613 changes in the relative abundance of heterohelicids (particularly *H. planata, H.*
614 *navarroensis* and *H. globulosa*) and increased *P. hariaensis* abundance in the >150 μm
615 fraction.
616 The end of the late Maastrichtian warming at Elles is marked by abrupt cooling
617 concurrent with unprecedented low MS values and increased test fragmentation ~4 m
618 below the KTB. This could be an expression of increased volcanic SO_2 emission and
619 acidification (Fig. 10 this study; Fig. 5 of Stüben et al., 2003). At Bidart the onset of this
620 same cooling event is recognized by a drop in MS associated with increased dissolution

and disappearance of *Globigerinelloides yaucoensis*, *P. costulata*, *G. subcarinatus* and *R. rugosa* and at Gamsbach the disappearance of *G. subcarinatus* (Figs. 8, 10).

8.2 Paleoproductivity

Low $\delta^{13}C$ values with multiple negative excursions are observed at Elles and Bidart (~0.5‰ and ~0.7‰ respectively) near the end of the late Maastrichtian CF1 warm event Fig. 7). Similar negative excursions (~1 ‰) are recorded at deep marine Site 525A (~0.3 ‰) as well as in shallow marine environments of Texas and India (Meghalaya) (Li and Keller, 1998a; Gertsch et al., 2011; Abramovich et al., 2011). The existing dataset shows a greater magnitude of $\delta^{13}C$ negative shift in the shallow sites (e.g., Meghalaya (India), Mullinax-1 (Texas) and slightly deeper Elles (Tunisia). The smaller $\delta^{13}C$ shift at deeper Site 525A may be due to an incomplete record resulting from erosion of early Danian and topmost Maastrichtian sediments (Li and Keller, 1998a).

A rise in sea level near the end of the Maastrichtian and across the KTB transition accompanied by increased precipitation and continental weathering/erosion (Haq et al., 1988; Li et al., 1999) may have been responsible for the increased delivery of organic carbon with very low $\delta^{13}C$ values into shallow marine environments. Low primary productivity could have been the other important contributor to the low $\delta^{13}C$ values. Low nannofossil productivity is recorded in Elles, Bidart, DSDP Site 525A, DSDP Site 577A and DSDP Site 216 during the late Maastrichtian warm event in CF1 (Gorostidi and Lamolda, 1995; Gardin, 2002; Tantawy et al., 2009; Thibault and Gardin, 2007, 2010). Heterotrophic planktic foraminifera may have in turn suffered, resulting in a decrease in carbonate export and the eventual $\delta^{13}C$ value of bulk carbonate. The lower carbonate

644 (40%) between 1.2-3.0 m below the KTB at Bidart, correlative with the low $\delta^{13}C$ interval
645 lends support to this interpretation.

646 These global effects of increased precipitation and enhanced continental
647 weathering/erosion can be attributed to climate warming caused by ongoing large scale
648 Deccan volcanism. Additionally, the outgassing of higher-than-background quantities of
649 volcanic CO_2 ($\delta^{13}C$ about -5‰) would also significantly contribute to lowering the $\delta^{13}C$
650 of the global oceans dissolved inorganic carbon (DIC), although the sediment record of
651 this signal would lag by ~1000 years (Zeebe, 2012).

652

653 **8.3 Planktic Foraminifera**

654 The high abundance of planktic and near absence of benthic foraminifera at Bidart
655 is consistent with the high planktic:benthic ratio (>90% planktics) reported by Coccioni
656 and Marsili (2007). The middle bathyal paleobathymetry and open marine setting appears
657 to be the reason for the unusual globotruncanid abundance at Bidart and Gamsbach (Fig.
658 9). This is supported by the high abundance of globotruncanids at Site 525A (~35-40%,
659 >150 μm) where deposition occurred at ~1000 m depth (Shackleton and Boersma, 1985;
660 Abramovich and Keller, 2003). In relatively shallow (<150 m) continental shelf
661 environments, such as Elles, the diversity and abundance of globotruncanids is much
662 lower (Fig. 9).

663

664 **8.4 Pre-KTB Ocean Acidification**

665 White et al. (1994) showed that under present-day conditions (pH rain=5.6),
666 magnetite grains have very long time residence (>10^7 years) on land, but can be rapidly

667 dissolved under more acidic conditions. In marine sediments, iron oxide dissolution by
668 ocean acidification has previously been documented for the Triassic-Jurassic mass
669 extinction and the coeval Central Atlantic Magmatic Province (Abrajevitch et al., 2013),
670 and more recently in the case of the KTB mass extinction at Bidart and Gubbio (Font et
671 al., 2014). The top ~50 cm interval of low-magnetic susceptibility (MS) that immediately
672 precedes the KTB at Bidart was attributed to the main phase-2 of Deccan volcanism
673 (Font et al., 2011, 2014; Font and Abrajevitch, 2014). The reductive iron oxide
674 dissolution may have occurred on land and/or in seawater. The first scenario was tested
675 by Font et al. (2014) who used a numerical weathering model to test for the consequences
676 of acidic rains on a continental regolith. Results revealed nearly complete magnetite
677 dissolution after ~31kyr (with a pH of 3.3.). However, the dissolution of magnetotactic
678 bacteria, which generally thrive the oxic-anoxic boundary in deep-sea marine sediments,
679 evokes ocean acidification as well and requires validation (Font and Abrajevitch, 2014;
680 Abrajevitch et al., in review).

681 Factors affecting the nature and concentration of detrital magnetic minerals and
682 therefore the MS of sediments include the nature and proximity of continental sediment
683 sources carbonate productivity, sea-level changes and/or post-depositional alteration
684 mechanisms (oxidation due to weathering/ diagenetic reduction of oxides). The influence
685 of sea level change on bulk MS is based on the relative contribution of carbonate
686 (diamagnetic, low MS) versus detrital input (paramagnetic clays and ferromagnetic iron
687 oxides, high MS) and thus can be estimated by correlating MS data with phyllosilicates
688 where a direct positive correlation implies a strong dependence of both parameters.

689 At Elles, the pre-KTB low-MS interval is not evident probably because

690 paramagnetic minerals (clays) dominate the MS signal, supported by very low Ca:detritus
691 ratios (Fig. 10). At Bidart, the correlation between percent phyllosilicates and MS in zone
692 CF1 is poor (r=0.088), indicating an overall weaker influence due to sea level changes or
693 turbidity currents. For Gamsbach, this correlation is more complicated due to the
694 presence of frequent turbidite beds that are rich in dia/paramagnetic-silicates (Fig. 10;
695 samples Gb 5, 10, 12, 15, 27-28). However, the MS profile of Gambsach does show low
696 MS values for the ~40 cm interval below the KTB, similar to the MS profile of the Bidart
697 section (Fig. 10). The MS data of the present study thus suggest that the Gambsach
698 section is a good analog of the Bidart section. A prolonged period of acid rain on the
699 continents resulting in dissolution of magnetic detrital minerals can therefore be the
700 principal mechanism that caused the low MS intervals antecedent to the KTB because sea
701 level changes are a secondary influence on the MS profiles of Bidart and Gamsbach,

702 Surface ocean acidification in the low MS intervals of Bidart and Gamsbach is
703 indicated by increased dissolution and fragmentation of planktic foraminiferal tests (Fig.
704 10). This increased fragmentation interval correlates with the abrupt cooling event at
705 Elles (~4 m to ~0.5 m below the KTB), Bidart (~0.5 m interval below the KTB) and
706 Gamsbach (~0.4 m interval below the KTB) despite their different paleogeography,
707 paleobathymetry, depositional conditions and faunal assemblages, suggesting a common
708 cause. An increase in the proportion of dissolved tests (in addition to physically
709 fragmented ones) in Bidart and Gamsbach confirm the contribution of chemical leaching
710 as cause for imperfect carbonate tests with holes. This implies that water column
711 acidification is a likely cause for the observed increase in FI.

712 Benthic foraminifera are well preserved and even pristine looking in the same

713 samples alongside leached and fragmented planktic foraminiferal tests at Bidart and
714 Gamsbach (Plates 2, 3). This may indicate acidification restricted to the upper water
715 column, or may reflect the inherently more robust mechanically resistant benthic tests.
716 Alegret et al. (2004; fig. 4) noted an increase in the proportion of agglutinated
717 foraminifera relative to calcareous benthic foraminifera in the top 10-cm of the
718 Maastrichtian at Bidart. We confirm these to be arenaceous (do not dissolve with 1:1
719 HCl), which may be interpreted as a consequence of ocean acidification or dissolution.
720 Only in the KTB red clay layer are benthic species corroded suggesting that low pH
721 acidic waters reached through the water column into deeper waters precisely at the KT
722 boundary event. However, the benthic species were little affected by the KTB mass
723 extinction or ocean acidification as their survival is globally documented (Widmark and
724 Malmgren, 1992; Alegret et al., 2001, 2003. Alegret and Thomas, 2004). For the most
725 part preceding the KTB, ocean acidification was restricted to the upper water column
726 with surface waters in equilibrium with very high atmospheric pCO_2 and low CO_3^{2-}
727 concentrations. Dissolution of test calcite during sinking through the water column would
728 make tests more fragile in post-depositional transport. The degree of
729 dissolution/fragmentation appears to be largely affected by local paleobathymetry and
730 species composition of the assemblage.

731 At Elles, the percentage of fragments is high throughout zone CF1 owing to
732 greater bottom water currents at shallower depths and also dominance of thin-walled
733 fragile heterohelicids in the assemblage (Fig. 10). In contrast, at Bidart the overall test
734 fragmentation is quite low due to a high proportion of structurally more robust
735 globotruncanids and quieter deposition at a greater depth. However, the proportion of

736 leached out tests with holes due to dissolution increased (Fig. 10; red). At Gamsbach, the
737 degree of fragmentation is high throughout zone CF1 despite a high abundance of
738 globotruncanids. This can be attributed to the frequent turbiditic activity at this site that
739 may have increased post-depositional transport and fragmentation. The variable lithology
740 (deposition of quartz rich beds/lenses) may have facilitated pore-water dissolution,
741 recrystallization-cementation leading to lithified sediments that are difficult to
742 disaggregate and free individual tests.
743
744 **8.5 Ocean acidification: The missing link to Deccan Volcanism?**
745 The main phase-2 of Deccan volcanism occurred over ~750kyr entirely within
746 chron C29r, straddling the KTB (Schoene et al., 2014). However, all volcanism did not
747 occur at uniform intensity within this interval, as inferred from the multiple eruptive
748 events of geologically short duration separated by red/green boles indicating periods of
749 quiescence (Subbarao et al., 2000; Jay and Widdowson, 2008; Chenet et al., 2007, 2008).
750 Four of the Deccan phase-2 longest lava-flows across the Indian sub-continent (likely
751 signifying peak volcanic activity) erupted within a duration of ~250 kyr (zone CF2-CF1)
752 as seen in the Krishna-Godavari basin, India. The overlying Danian zone P1a sediments
753 constrain the age of the KTB mass extinction as coincident with the final mega-flow of
754 the peak phase-2 eruptions. (Keller et al., 2011a, 2012). The resultant cumulative loading
755 of 12,000–28,000 Gigatons (Gt) of CO_2 into the end Cretaceous atmosphere within tens
756 of thousand years could increase the pCO_2 on timescales that are recorded in the
757 sediments. This excess CO_2 equilibrates with surface ocean water thus altering the
758 carbonate chemistry. The carbonic acid (H_2CO_3) formed dissociates to bicarbonate anion

759 (HCO^-_3) and H^+ ions, reducing the pH of surface waters. These H^+ ions combine with
760 CO_3^{2-} anions forming more HCO_3^- and decreasing the bioavailability of CO_3^{2-} to
761 calcifying organisms to build their tests.

762 The episodic release of hundreds to thousands of teragrams of volcanogenic SO_2
763 per year for each Deccan eruption would form sulfate aerosols upon reaction with
764 atmospheric water vapor and precipitate out as toxic acid rain locally/regionally
765 centennial timescales, shorter than the millennial timescales for removal of CO_2 (Self et
766 al., 2008; Chenet et al., 2009; Mussard et al., 2014; Callegaro et al., 2014). This could
767 have been directly toxic/lethal for continental flora and fauna of affected areas. On land,
768 acid rain would exacerbate continental weathering. Sulfur dioxide would also lower the
769 surface ocean pH further, significantly contributing to the calcification crisis and high-
770 stress conditions for calcifying organisms on shorter timescales.

771 Ocean acidification has been identified as an important mechanism associated
772 with faunal turnovers and mass extinction events through geological history (e.g. ocean
773 anoxic events (OAEs) of the Paleozoic and the Paleocene-Eocene thermal maximum
774 (PETM)) that have affected marine calcifiers e.g. coccolithophores, planktic and benthic
775 foraminifera (review in Hönisch et al., 2012). Physiological manifestations of high-stress
776 due to acidification recorded as dwarfism, deformed tests, and R- strategist–dominated
777 assemblages in the Late Maastrichtian have already been linked with phase-2 Deccan
778 volcanism (Erba et al., 2010; review in Punekar et al., 2014a). Moy et al. (2009) reported
779 a 30%–35% lower calcification in modern *Globigerina bulloides* from the Southern
780 Ocean as compared to Holocene specimens. The anthropogenic CO_2 emissions have
781 resulted in acidification of the Southern Ocean in the past ~300 yr (drop in pH by 0.1

782 units, expected drop of 0.7 units in the next ~300 yr; Orr et al., 2005; Zeebe et al., 2008).
783 Carbonate tests of planktic organisms can experience dissolution in the water column as
784 demonstrated by the *in vitro* pteropod shell dissolution within 48 hours of exposure to
785 low pH waters (Fabry et al., 2008; Doney et al., 2009). The cumulative effect of thinner
786 walled tests undergoing water-column dissolution can render a test increasingly fragile
787 and vulnerable to fragmentation, consistent with our taphonomic evidence for ocean
788 acidification.

789 There are multiple lines of evidence in support of global surface ocean
790 acidification associated with the main phase-2 Deccan volcanism: (1) intensely corroded
791 carbonate tests and rapid extinctions of Maastrichtian planktic foraminifera in the
792 intertrappean sediments of the lava mega-flows in the Krishna-Godavari Basin of India
793 (Keller et al., 2011a, 2012). (2) Strong carbonate dissolution and high-stress
794 environments indicated by intense *Guembelitria* blooms (>95%) in CF1 of Meghalaya
795 (NE India) (Gertsch et al., 2011). And (3) evidence for iron oxide dissolution by
796 acidification inferred from low MS as well as for surface ocean acidification near the end
797 of zone CF1 preceding the KTB at distal sites such as Bidart (France) and Gamsbach
798 (Austria) as documented in this study.

799

800 **9. Conclusions**

801 Good temporal correlation between the age of the main phase of Deccan volcanic
802 eruptions in India and the age and episodic nature of climate fluctuations worldwide has
803 strengthened the case for large scale volcanism as a significant contributor to the Late
804 Maastrichtian biotic stress that culminated in the KTB mass extinction. However,

inherent limitations due to incompleteness of the stratigraphic record and the lack of a convincing kill-mechanism have inspired strong skepticism for this hypothesis.

A multi-proxy study of the Late Maastrichtian zone CF1 in Bidart (France) and Gamsbach (Austria) reveals events in the final ~160 ky of the Late Maastrichtian that are critical to understanding the role of Deccan volcanism in global high stress environments and leads to the following conclusions.

- The Late Maastrichtian warm event in the lower part of zone CF1 at Bidart (France) and Gamsbach (Austria) is recognized by faunal responses similar to those observed at Elles (Tunisia) and DSDP Site 525A.
- A period of low $\delta^{13}C$ values and decreased percent $CaCO_3$ content during the global warming may record a combination of increased continental ^{12}C influx through increased runoff, suppressed primary and calcifier productivity and equilibration of surface ocean waters with increased isotopically lighter volcanogenic CO_2.
- An increase in carbonate dissolution and foraminiferal test fragmentation suggests surface ocean acidification in 60-cm immediately preceding the KTB at Bidart (France) and Gamsbach (Austria). This event globally correlates with the low MS interval defined as the Deccan benchmark interval in Bidart by Font et al., (2011, 2014).
- The widespread ocean acidification interval is coincident with the rapid cooling. At Elles, evidence for another rapid warming following this interval coincides with the KTB mass extinction. The acidification may be the result of equilibration with huge amounts of CO_2 injected rapidly into the

atmosphere at rates overwhelming the response time of feedback mechanisms.

Acknowledgements:

This research was supported by Princeton University's Scott and Tuttle Funds, the U.S. National Science Foundation (grants NSF EAR-0207407, EAR-0447171 and EAR-1026271) and FCT (ref. PTDC/CTE-GIX/117298/2010). We thank the three anonymous reviewers and the Guest Editor Prof. Wolfram M. Kürschner for their insightful comments and suggestions.

REFERENCES

Abrajevitch, A., Hori, R. S., and Kodama, K., 2013. Rock magnetic record of the Triassic-Jurassic transition in pelagic bedded chert of the Inuyama section, Japan. Geology, 41(7), 803-806.

Abramovich, S. and Keller, G., 2002. High stress late Maastrichtian paleoenvironment: inference from planktonic foraminifera in Tunisia. Palaeogeography, Palaeoclimatology, Palaeoecology, 178(3), 145-164. doi: 10.1016/S0031-0182(01)00394-7

Abramovich, S. and Keller, G., 2003. Planktonic foraminiferal response to the latest Maastrichtian abrupt warm event: a case study from South Atlantic DSDP Site

525A. Marine Micropaleontology, 48(3), 225-249. 10.1016/S0377-8398(03)00021-5

Abramovich, S., Keller, G., Berner, Z., Cymbalista, M., and Rak, C., 2011. Maastrichtian Planktic Foraminiferal Biostratigraphy and Paleoenvironment of Brazos River, Falls County, Texas, in: Keller, G. and Adatte ,T., eds., 100 SEPM Special Publication, 123–156. doi: 10.1017/S0016756812001069

Abramovich, S., Keller, G., Stüben, D. and Berner, Z., 2003. Characterization of late Campanian and Maastrichtian planktonic foraminiferal depth habitats and vital activities based on stable isotopes. Palaeogeography, Palaeoclimatology, Palaeoecology, 202(1), 1-29. 10.1016/S0031-0182(03)00572-8

Abramovich, S., Yovel-Corem, S., Almogi-Labin, A. and Benjamini, C., 2010. Global climate change and planktic formaminiferal response in the Maastrichtian: Paleoceanography, 25, PA2201. doi:10.1029/2009PA001843.

Adatte, T., Keller, G. and Stinnesbeck, W., 2002. Late Cretaceous to early Paleocene climate and sea-level fluctuations. Paleogeography, Paleoclimatology, Paleoecology, 178, 165-198. doi: 10.1016/S0031-0182(01)00395-9

Adatte, T., Keller, G., Stüben, D., Harting, M., Kramar, U., Stinnesbeck, W., Abramovich, S. and Benjamini, C., 2005. Late Maastrichtian and K/T

873 paleoenvironment of the eastern Tethys (Israel): mineralogy, trace element and
874 platinum group elements, biostratigraphy and faunal turnovers. Bulletin Société
875 Géologique de France, 176(1), 35-53. doi: 10.2113/176.1.37
876
877 Adatte, T., Stinnesbeck, W. and Keller, G. 1996. Lithostratigraphic and mineralogic
878 correlations of near K/T boundary sediments northeastern Mexico: implications
879 for origin and nature of deposition. The Cretaceous–Tertiary Event and Other
880 Catastrophes in Earth History, Boulder, Colorado. Geological Society of America
881 Special Papers, 307, 211–226.
882
883 Alegret, L. and Thomas, E., 2004. Benthic foraminifera and environmental turnover
884 across the Cretaceous/Paleogene boundary at Blake Nose (ODP Hole 1049C,
885 Northwestern Atlantic). Palaeogeography, Palaeoclimatology, Palaeoecology,
886 208(1), 59-83. doi: 10.1016/j.palaeo.2004.02.028
887
888 Alegret, L., Kaminski, M. A. and Molina, E., 2004. Paleoenvironmental recovery after
889 the Cretaceous/Paleogene boundary crisis: evidence from the marine Bidart
890 section (SW France). Palaios, 19(6), 574-586. doi: 10.1669/0883-
891 1351(2004)019<0574:PRATPB>2.0.CO;2
892
893 Alegret, L., Molina, E. and Thomas, E., 2001. Benthic foraminifera at the Cretaceous-
894 Tertiary boundary around the Gulf of Mexico. Geology, 29(10), 891-894. doi:
895 10.1130/0091-7613(2001)029<0891:BFATCT>2.0.CO;2

Alegret, L., Molina, E. and Thomas, E., 2003. Benthic foraminiferal turnover across the Cretaceous/Paleogene boundary at Agost (southeastern Spain): paleoenvironmental inferences. Marine Micropaleontology, 48(3), 251-279. doi: 10.1016/S0377-8398(03)00022-7

Apellaniz, E., Baceta, J. I., Bernaola-Bilbao, G., Núñez-Betelu, K., Orúe-Etxebarría, X., Payros, A., Pujalte, V., Robin, E. and Rocchia, R., 1997. Analysis of uppermost Cretaceous–lowermost Tertiary hemipelagic successions in the Basque Country (western Pyrenees): evidence for a sudden extinction of more than half planktic foraminifer species at the K/T boundary. Bulletin de la Societé Géologique de France, 168, 783–793.

Arenillas, I., Arz, J. and Molina, E., 2004. A new high-resolution planktic foraminiferal zonation and subzonation for the lower Danian. Lethaia, 37(1), 79-95. doi: 10.1080/00241160310005097

Arz, J. A. and Arenillas, I., 1998. Extinción en masa catastrófica de foraminíferos planctónicos en el límite Cretácico/Terciario del Pirineo occidental (España). Sociedad Mexicana de Paleontología Revista, 8(2), 146-162. doi: 10.1155/2013/643278

Arz, J. A. and Molina, E., 2002. Late Campanian and Maastrichtian biostratigraphy and chronostratigraphy based on planktic foraminifera in temperate and subtropical

latitudes (Spain, France and Tunisia). Neues Jahrbuch fur Geologie und Palaontologie-Abhandlungen, 224(2), 161-195.

Berger, W. H., Bonneau, M. C. and Parker, F. L., 1982. Foraminifera on the deep-sea floor-lysocline and dissolution rate. Oceanologica Acta, 5(2), 249-258.

Berggren, W.A., Kent, D.V., Swisher, C.C. and Aubry, M. P. 1995. A revised Cenozoic geochronology and chronostratigraphy. In: Berggren, W.A., Kent, D.V., Aubry, M. P., Hardenbol, J., eds., Geochronology, Time Scales and Global Stratigraphic Correlation. SEPM Special Publication 54, 129-212. doi: 10.2110/pec.95.04.0129

Bonté, P., Delacotte, O., Renard, M., Laj, C., Boclet, D., Jehanno, C., and Rocchia, R., 1984. An iridium rich layer at the Cretaceous/Tertiary boundary in the Bidart section (southern France). Geophysical Research Letters, 11(5), 473-476. doi: 10.1029/GL011i005p00473

Callegaro, S., Baker, D. R., De Min, A., Marzoli, A., Geraki, K., Bertrand, H., Viti, C., and Nestola, F., 2014. Microanalyses link sulfur from large igneous provinces and Mesozoic mass extinctions. Geology, 42(10), 895-898. doi: 10.1130/G35983.1

Cande, S. and Kent, D.V. 1995. Revised calibration of the geomagnetic polarity Timescale for the Late Cretaceous and Cenozoic. Journal of Geophysical Research, 100, 6093-6095. doi: 10.1029/94JB03098

Caron, M., 1985. Cretaceous planktic foraminifera. In: Bolli, H.M., Saunders, J.B. and Perch-Nielsen, K., eds. Plankton Stratigraphy: Cambridge, Cambridge University Press, 17-86.

Chenet, A. -L., Fluteau, F., Courtillot, V., Gérard, M., and Subbarao, K. V., 2008. Determination of rapid Deccan eruptions across the Cretaceous-Tertiary boundary using paleomagnetic secular variation: Results from a 1200-m-thick section in the Mahabaleshwar escarpment. Journal of Geophysical Research, 113(B4). doi: 10.1029/2006JB004635

Chenet, A., -L, Quidelleur, X., Fluteau, F., Courtillot, V., and Bajpai, S., 2007. 40K–40Ar dating of the Main Deccan large igneous province: Further evidence of KTB age and short duration. Earth and Planetary Science Letters, 263(1-2), 1-15. doi: 10.1016/j.epsl.2007.07.011

Clauser, S., 1994. Etudes stratigraphiques du Campanien et du Maastrichtien de l'Europe Occidentale: Cote Basque, Charentes (France), Limbourg (Pays-Bas). Documents du Bureau de Recherches Géologiques et Minières, 235, 243.

Coccioni, R. and Marsili, A., 2007. The response of benthic foraminifera to the K–Pg boundary biotic crisis at Elles (northwestern Tunisia). Palaeogeography, Palaeoclimatology, Palaeoecology, 255(1), 157-180. doi:10.1016/j.palaeo.2007.02.046

964 Cowie , J. W., Ziegler, W. and Remane , J., 1989. Stratigraphic Commission accelerates
965 progress, 1984 to 1989. Episodes, 12, 79-83.
966
967 Dekkers, M. J., 1997. Environmental magnetism: an introduction. Geologie en
968 Mijnbouw, 76(1-2), 163-182.
969
970 Delacotte, O., 1982. Etude magnétostratigraphique et géochimique de la limite Crétacé-
971 Tertiaire de la coupe de Bidart (Pyrennées Atlantiques). PhD thesis. Université
972 Pierre et Marie Curie, Paris, France.
973
974 Doney, S.C., Fabry, V.J., Feely, R.A., and Kleypas, J.A., 2009. Ocean acidifi cation:
975 The other CO2 problem. Annual Review of Marine Science, 1, 169–192,
976 doi:10.1146/annurev.marine.010908.163834.
977
978 Egger, H., Koeberl, C., Wagreich, M., and Stradner, H., 2009. The Cretaceous-Paleogene
979 (K/Pg) boundary at Gams, Austria: Nannoplankton stratigraphy and geochemistry
980 of a bathyal northwestern Tethyan setting. Stratigraphy, 6(4), 333-347.
981
982 Egger, H., Rögl, F., and Wagreich, M., 2004. Biostratigraphy and facies of Paleogene
983 deep-water deposits at Gams (Gosau Group, Austria) Annalen des
984 Naturhistorischen Museums Wien, 106A, 281–307.
985

Ellwood, B., MacDonald, W., Wheeler, C. and Benoist, S., 2003. The K–T boundary in Oman: identified using magnetic susceptibility field measurements with geochemical confirmation. Earth and Planetary Science Letters, 206(3), 529-540. doi:10.1016/j.palaeo.2008.01.005

Ellwood, B., Tomkin, J., Ratcliffe, K., Wright, M., and Kafafy, A., 2008. High-resolution magnetic susceptibility and geochemistry for the Cenomanian/Turonian boundary GSSP with correlation to time equivalent core. Palaeogeography, Palaeoclimatology, Palaeoecology, 261(1), 105-126. doi:10.1016/j.palaeo.2008.01.005

Erba, E., Bottini, C., Weissert, H.J., and Keller, C.E., 2010. Calcareous nannoplankton response to surface-water acidification around oceanic anoxic event 1a. Science, 329(5990), 428–432, doi:10.1126/science.1188886.

Erbacher, J., Mosher, D. C. and Malone, M. J., 2004. Demerara Rise: Equatorial Cretaceous and Paleogene Paleoceanographic Transect, Western Atlantic. In Proceedings of the Ocean Drilling Program, Initial Reports, 207.

Fabry, V.J., Seibel, B.A., Feely, R.A., and Orr, J.C., 2008. Impacts of ocean acidification on marine fauna and ecosystem processes: ICES Journal of Marine Science: Journal du Conseil, 65(3), 414–432. doi:10.1093/icesjms/fsn048.

1009 Font, E. and Abrajevitch, A., 2014. Paleoenvironmental signature of the Deccan Phase 2.
1010 Frontiers in Earth Sciences. doi: 10.3389/feart.2014.0002.
1011
1012 Font, E., Nedelec, A., Ellwood, B.B., Mirao, J., and Silva, P.F., 2011. A new sedimentary
1013 benchmark for the Deccan Traps volcanism? Geophysical Research Letters, 38,
1014 L24309. doi: 10.1029/2011GL049824
1015
1016 Font, E., Fabre, S., Nédélec, A., Adatte, T., Keller, G., Veiga-Pires, C., Ponte, J., Mirão,
1017 J., Khozyem, H., and Spangenberg, J. E., 2014. Atmospheric halogen and acid
1018 rains during the main phase of Deccan eruptions: Magnetic and mineral
1019 evidence. Geological Society of America Special Papers, 505, SPE505-18. doi:
1020 10.1130/2014.2505(18)

1021 Galbrun, B., and Gardin, S., 2004. New chronostratigraphy of the Cretaceous –Paleogene
1022 boundary interval at Bidart (France). Earth and Planetary Science Letters, 224,
1023 19-32. doi: 10.1016/j.epsl.2004.04.043

1024 Gallala, N., 2013. Planktonic Foraminiferal Biostratigraphy and Correlation Across the
1025 Cretaceous-Paleogene Transition at the Tethyan and the Atlantic Realms.
1026 Paleontology Journal, 2013.

1027 Gallala, N., Zaghbib-Turki, D., Arenillas, I., Arz, J. A., and Molina, E., 2009.
1028 Catastrophic mass extinction and assemblage evolution in planktic foraminifera
1029 across the Cretaceous/Paleogene (K/Pg) boundary at Bidart (SW France). Marine
1030 Micropaleontology, 72(3), 196-209. doi: 10.1016/j.marmicro.2009.05.001

Gardin, S., 2002. Late Maastrichtian to early Danian calcareous nannofossils at Elles (Northwest Tunisia). A tale of one million years across the K–T boundary. Palaeogeography, Palaeoclimatology, Palaeoecology, 178(3), 211-231.

Georgescu, M. D. and Abramovich, S., 2009. A new Late Cretaceous (Maastrichtian) serial planktic foraminifer (Family Heterohelicidae) with early planispiral coil and revision of *Spiroplecta* Ehrenberg, 1844. Geobios, 42(6), 687-698.

Gertsch, B., Keller, G., Adatte, T., Garg, R., Prasad, V., Berner, Z., and Fleitmann, D., 2011. Environmental effects of Deccan volcanism across the Cretaceous–Tertiary transition in Meghalaya, India. Earth and Planetary Science Letters, 310(3-4), 272-285. doi: 10.1016/j.epsl.2011.08.015

Grachev, A.F. (ed.), 2009. The K/T boundary of Gams (Eastern Alps, Austria) and the nature of terminal Cretaceous mass extinction. Vienna (Geologische Bundesanstalt), 199. doi: 10.2205/2009-GAMSbook

Grachev, A. F., Korchagin , O. A., Kollmann , H. A., Pechersky, D. M. and Tsel ´movich, V. A., 2005. A new look at the nature of the transitional layer at the K/T boundary near Gams, Eastern Alps, Austria, and the problem of the mass extinction of the biota. Russian Journal of Earth Sciences, 7: doi: 10.2205/2005ES000189.

1053 Gradstein , F., Ogg , J. and Smith , A., 2004. A Geologic Time Scale 2004. Cambridge:
1054 Cambridge University Press, 589.
1055
1056 Gorostidi, A., and Lamolda, M. A., 1995. La nannoflora calcárea y el tránsito KT de la
1057 sección de Bidart (SW de Francia). Revista Española de Paleontología no.
1058 Homenaje al Dr. Guillermo Colom, 153–168.
1059
1060 Grachev, A. F., Borisovsky, S. E., and Grigor'eva, A. V., 2008. The first find of native
1061 rhenium in the transitional clay layer at the Cretaceous/Paleogene boundary in the
1062 Gams Section (eastern Alps, Austria). In Doklady Earth Sciences, 422(1), 1065-
1063 1067. MAIK Nauka/Interperiodica. doi: 10.1134/S1028334X08070131
1064
1065 Grachev, A. F., Korchagin, O. A., Kollmann, H. A., Pechersky, D. M. and Tsel'movich,
1066 V. A., 2005. A new look at the nature of the transitional layer at the K/T boundary
1067 near Gams, Eastern Alps, Austria, and the problem of the mass extinction of the
1068 biota. Russian Journal of Earth Sciences, 7(6).
1069
1070 Haslett, S.K., 1994. Planktonic foraminiferal biostratigraphy and palaeoceanography of
1071 the Cretaceous–Tertiary boundary section at Bidart, south–west France,
1072 Cretaceous Research, 15, 179–192. doi: 10.1006/cres.1994.1009
1073
1074 Haubold , H., Scholger, R., Frisch , W., Summesberger, H. and Mauritsch , H. J., 1999.
1075 Reconstruction of the geodynamic evolution of the Northern Calcareous Alps by

means of paleomagnetism. Physics and Chemistry of the Earth, Part A: Solid Earth and Geodesy (A), 24, 697-703. doi: 10.1016/S1464-1895(99)00101-5

Hönisch, B., Ridgwell, A., Schmidt, D.N., Thomas, E., Gibbs, S.J., Sluijs, A., Zeebe, R., Kump, L., Martindale, R.C., Greene, S.E., Kiessling, G., Ries, J., Zachos, J.C., Royer, D.L., Barker, S., Marchitto, T.M., Jr., Moyer, R., Pelejero, C., Ziveri1, P., Foster, G.L., and Williams, B., 2012. The geological record of ocean acidifi cation, Science, 335(6072), 1058–1063. doi:10.1126/science.1208277.

Jay, A. E. and Widdowson, M., 2008. Stratigraphy, structure and volcanology of the SE Deccan continental flood basalt province: implications for eruptive extent and volumes. Journal of the Geological Society, 165(1), 177-188. doi: 10.1144/0016-76492006-062

Keller, G., 2004. Paleoecology of Late Maastrichtian-early Danian planktic foraminifera in the eastern Tethys. Journal of Foraminiferal Research, 34(1), 49-73.

Keller, G. and Benjamini, C., 1991. Paleoenvironment of the eastern Tethys in the early Danian, Palaios, 6, 439-464. doi: 10.2307/3514984

Keller, G., Abramovich, S., Adatte, T., and Berner, Z., 2011b, Biostratigraphy, age of the Chicxulub impact, and depositional environment of the Brazos River KTB sequences, in Keller, G., and Adatte, T., eds., The End-Cretaceous Mass

1099 Extinction and the Chicxulub Impact in Texas: Society for Sedimentary Geology
1100 (SEPM) Special Publication 100, 81–122.

1101 Keller, G., Abramovich, S., Berner, Z., and Adatte, T., 2009. Biotic effects of the
1102 Chicxulub impact, K-T catastrophe and sea-level change in Texas.
1103 Paleogeogeography, Paleoclimatology, Paleoecology, 271, 52-68. doi:
1104 10.1016/j.palaeo.2008.09.007
1105
1106 Keller, G., Adatte, T., Bhowmick, P. K., Upadhyay, H., Dave, A., Reddy, A. N., and
1107 Jaiprakash, B. C., 2012. Nature and timing of extinctions in Cretaceous-Tertiary
1108 planktic foraminifera preserved in Deccan intertrappean sediments of the
1109 Krishna–Godavari Basin, India. Earth and Planetary Science Letters, 341, 211-
1110 221. doi: 10.1016/j.epsl.2012.06.021
1111
1112 Keller, G., Adatte, T., Burns, S. J., Tantawy, A. A., 2002a. High-stress paleoenvironment
1113 during the late Maastrichtian to early Paleocene in central Egypt.
1114 Palaeogeography, Palaeoclimatology, Palaeoecology 187, 35e60. doi:
1115 10.1016/S0031-0182(02)00504-7
1116
1117 Keller, G., Adatte, T., Stinnesbeck, W., Luciani, V., Karoui, N. and Zaghbib-Turki, D.,
1118 2002b. Paleoecology of the Cretaceous-Tertiary mass extinction in planktic
1119 foraminifera. Paleogeography, Paleoclimatology, Paleoecology, 178, 257-298.
1120 doi: 10.1016/S0031-0182(01)00399-6
1121

1122 Keller, G., Adatte, T., Stinnesbeck, W., Stuben, D. and Berner, Z. 2001. Age, chemo-
1123 and biostratigraphy of Haiti spherule-rich deposits: a multi-event K-T scenario.
1124 Canadian Journal of Earth Sciences, 38, 197-227. doi: 10.1139/e00-087
1125
1126 Keller, G., Adatte, T., Stinnesbeck, W., Stüben, D., Kramar, U., Berner, Z., Li, L. and
1127 Perch-Nielsen, K. V. S., 1997. The Cretaceous-Tertiary transition on the shallow
1128 Saharan platform of southern Tunisia. Geobios, 30(7), 951-975.
1129
1130 Keller, G., Adatte, T., Tantawy, A. A., Berner, Z., and Stüben, D., 2007. High Stress Late
1131 Cretaceous to early Danian paleoenvironment in the Neuquen Basin, Argentina.
1132 Cretaceous Research, 28, 939-960. doi: 10.1016/j.cretres.2007.01.006
1133

1134 Keller, G., Bhowmick, P. K., Upadhyay, H., Dave, A., Reddy, A. N., Jaiprakash, B. C. and
1135 Adatte, T., 2011a. Deccan Volcanism Linked to the Cretaceous-Tertiary Boundary Mass
1136 Extinction : New Evidence from ONGC Wells in the Krishna-Godavari Basin. Journal of
1137 the Geological Society of India, 78, 399-428. doi: 10.1007/s12594-011-0107-3.

1138 Keller, G., Khozyem, H., Adatte, T., Malarkodi, N., Spangenberg, J. E. and Stinnesbeck,
1139 W., 2013. Chicxulub impact spherules in the North Atlantic and Caribbean: age
1140 constraints and Cretaceous–Tertiary boundary hiatus. Geological Magazine,
1141 150(05), 885-907.
1142

1143 Keller, G., Li, L. and MacLeod, N., 1995. The Cretaceous/Tertiary boundary stratotype section at
1144 El Kef, Tunisia: How catastrophic was the mass extinction? Paleogeography,
1145 Paleoclimatology, Paleoecology, 119, 221-254. doi: 10.1016/0031-0182(95)00009-7
1146
1147 Keller, G., Lyons, J.B., MacLeod, N., and Officer, C.B., 1993. Is there evidence for
1148 Cretaceous-Tertiary boundary impact deposits in the Caribbean and Gulf of
1149 Mexico? Geology, 21, 776-780. doi: 10.1130/0091-7613(1993)
1150
1151 Keller, G., Stinnesbeck, W., Adatte, T. and Stüben, D., 2003. Multiple Impacts across the
1152 Cretaceous-Tertiary boundary. Earth Science Reviews, 62, 327-363. doi:
1153 10.1016/S0012-8252(02)00162-9
1154
1155 Kuiper, K. F., Deino , A., Hilgen , F. J., Krijgsman , W., Renne , P. R. and Wijbrans , J.
1156 R., 2008. Synchronizing rock clocks of Earth history. Science, 320, 500-504. doi:
1157
1158 10.1126/science.1154339
1159
1160
1161 Le, J., and Shackleton, N. J., 1992. Carbonate dissolution fluctuations in the western
1162 equatorial Pacific during the late Quaternary. Paleoceanography, *7*(1), 21-42.
1163
1164 Li, L. and Keller, G., l998a. Maastrichtian climate, productivity and faunal
1165 turnovers in planktic foraminifera in South Atlantic DSDP Sites 525A and 21,
1166 Marine Micropaleontology, 33, 55-86. doi: 10.1016/S0377-8398(97)00027-3
1167

Li, L. and Keller, G., l998b. Diversification and extinction in Campanian-Maastrichtian planktic foraminifera of northwestern Tunisia. Eclogae Geologicae Helveticae, 91, 75-102. doi: 0012-9402/98/010075-28

MacLeod, N. and Keller, G., 1991. Hiatus distributions and mass extinctions at the Cretaceous/Tertiary boundary, Geology, 19, 497-501. doi: 10.1016/0031-0182(95)00009-7

Malmgren, B. A., 1987. Differential dissolution of Upper Cretaceous planktonic foraminifera from a temperate region of the South Atlantic Ocean. Marine Micropaleontology, 11(4), 251-271.

Moore, J. C., Klaus, A. and Bangs, N.L., 1998. Site 1049, Proc. ODP, Initial Reports 171A (1998), 47–91.

Moy, A.D., Howard, W.R., Bray, S.G., and Trull, T.W., 2009. Reduced calcification in modern Southern Ocean planktonic foraminifera. Nature Geoscience, 2(4), 276–280. doi:10.1038/ngeo460.

Mussard, M., Le Hir, G., Fluteau, F., Lefebvre, V., and Goddéris, Y., 2014, Modeling the carbon-sulfate interplays in climate changesrelated to the emplacement of continental flood basalts, in Keller, G., and Kerr, A.C., eds., Volcanism, Impacts,

and Mass Extinctions: Causes and Effects. Geological Society of America Special Paper 505, doi: 10.1130/2014.2505(17).

Nederbragt, A. J., 1991. Late Cretaceous biostratigraphy and development of Heterohelicidae (planktic foraminifera). Micropaleontology, 329-372. 10.2307/1485910

Nelson, B.K., Macleod, G.K. and Ward, P.D., 1991. Rapid change in strontium isotopic composition of seawater before the Cretaceous/Tertiary boundary. Nature, 351, 644–647. doi: 10.1038/351644a0

Olsson, R.K., Hemleben, C., Berggren, W.A. and Huber, B.T., 1999. Atlas of Paleocene Planktonic Foraminifera. Smithsonian Contribution to Paleobiology No. 85. Smithsonian Institution Press, Washington D.C., pp. 252.

Orr, J.C., Fabry, V.J., Aumont, O., Bopp, L., Doney, S.C., Feely, R.A., Gnanadesikan, A., Gruber, N., Ishida, A., Joos, F., Key, R.M., Lindsay, K., Maier-Reimer, E., Matear, R., Monfray, P., Mouchet, A., Najjar, R.G., Plattner, G-K., Rodgers, K.B., Sabine, C.L., Sarmiento, J.L., Schlitzer, R., Slater, R.D., Totterdell, I.J., Weirig, M-F., Yamanaka, Y., and Yool, A., 2005. Anthropogenic ocean acidification over the twenty-first century and its impact on calcifying organisms. Nature, 437, 681–686. doi:10.1038/nature04095.

Pechersky, D. M., Grachev, A. F., Nourgaliev, D. K., Tsel'movich, V. A. and Sharonova, Z. V., 2006. Magnetolithologic and magnetomineralogical characteristics of deposits at the Mesozoic/Cenozoic boundary: Gams section (Austria). Russian Journal of Earth Sciences, 8(3). doi: 10.2205/2006ES000204.

Peybernes, B., Fondecave-Wallez, M.J., Gourinard, Y., and Eichène, P., 1997. Stratigraphie séquentielle comparée et grade-datation par les foraminifères planctoniques du Campano-Maastrichtien et du Paléocène de quelques sites d'Europe sud-occidentale et d'Afrique du Nord Comptes Rendus de l'Académie des Sciences, Series D, Sciences de la Terre, 324, 839–846. doi: 10.1016/S1251-8050(97)82519-0

Pueyo, E. L., Mauritsch , H. J., Gawlick , H. -J., Scholger, R. and Frisch , W., 2007. New evidence for block and thrust sheet rotations in the central northern Calcareous Alps deduced from two pervasive remagnetization events. Tectonics, 26, TC5011, doi: 10.1029/2006TC001965.

Punekar, J., Keller, G., Khozyem, H., Hamming, C., Adatte, T., Tantawy, A. A. and Spangenberg, J. E. 2014b. Late Maastrichtian–early Danian high-stress environments and delayed recovery linked to Deccan volcanism. Cretaceous Research, 49, 63-82. 10.1016/j.cretres.2014.01.002

1236 Punekar, J., Mateo, P., and Keller, G., 2014a. Effects of Deccan volcanism on
1237 paleoenvironment and planktic foraminifera: A global survey. Geological Society
1238 of America Special Papers, 505, 91-116. doi: 10.1130/2014.2505(04)
1239
1240 Raja Rao, C.S., Sahasrabudhe, S.S., Deshmukh, S.S. and Raman, R. 1999. Distribution,
1241 structure and petrography of the Deccan Traps, India, in: K.V. Subbarao (Ed.),
1242 Deccan Volcanic Province, Memoir - Geological Society of India, 43, 401–414.
1243
1244 Razin, P., 1989. Evolution tectono-sédimentaire alpine des Pyrénées Basques à l'Ouest de
1245 la transformante de Pampelune (Province du Labourd) (Thèse de
1246 doctorat) Université de Bordeaux III, 464.
1247
1248 Renne, P. R., Deino, A. L., Hilgen, F. J., Kuiper, K. F., Mark, D. F., Mitchell, W. S.,
1249 Morgan, L. E., Mundil, R. and Smit, J., 2013. Time scales of critical events
1250 around the Cretaceous-Paleogene boundary. Science, 339(6120), 684-687. doi:
1251 10.1126/science.1230492
1252
1253 Remane, J., Keller, G., Hardenbol, J., and Ben Haj Ali, M., l999. Report on the
1254 International Workshop on Cretaceous-Paleogene Transitions: Episodes, 22(1),
1255 47-48.
1256
1257 Renard, M., Delacotte, O., and Létolle, R., 1982. Le strontium et les isotopes stables
1258 dans les carbonates totaux de quelques sites de l'Atlantique et de la Tethys.

Bulletin de la Société Géologique de France, 14, 519–534. doi: 10.2113/gssgfbull.S7-XXIV.3.519

Robaszynski, F., Caron, M., Gonzalez-Donoso, J. M., Wonders, A. H., Ewgpf 1983–1984. Paris Atlas of late Cretaceous Globotruncanids. Revue de Micropaléontologie, 36 (3–4), 145–305.

Rocchia, R., Boclet, D., Bonté, Ph., Devineau, J., Jéhanno, C. and Renard, M., 1987. Comparaison des distributions de l'iridium observéesàla limite Crétacé-Tertiaire dans divers sites européens. Mémoires de la Société géologique de France N.S., 150 (1987), 95–103.

Rocchia, R., Robin, E., Froget, L. and Gayraud, J. 1996. Stratigraphic distribution of extraterrestrial markers at the Cretaceous-Tertiary boundary in the Gulf of Mexico area: Implications for the temporal complexity of the event. Geological Society of America, Special Paper, 307, 279-286.

Schöbel, S., de Wall, H., Ganerød, M., Pandit, M. K., and Rolf, C., 2014. Magnetostratigraphy and 40Ar–39Ar geochronology of the Malwa Plateau region (Northern Deccan Traps), central western India: Significance and correlation with the main Deccan Large Igneous Province sequences. Journal of Asian Earth Sciences, 89, 28-45. doi: 10.1016/j.jseaes.2014.03.022

1282 Schoene, B., Samperton, K., Eddy, M., Keller, G., Adatte, T., Bowring, S., Khadri, S. F.
1283 R. and Gertsch, B., 2014. U-Pb geochronology of the Deccan Traps and relation
1284 to the end-Cretaceous mass extinction. Science (aaa0118).
1285 doi:10.1126/science.aaa0118
1286
1287 Shackleton, N. and Boersma, A., 1985. History of the Walvis Ridge. A précis of the
1288 results of DSDP Leg 74 In: Moore, T. C. Jr, Rabinowitz, P. D. and Borella, P. E.,
1289 eds., South Atlantic Paleoceanography, 57.
1290
1291 Self, S., Blake, S., Sharma, K., Widdowson, M., and Sephton, S., 2008. Sulfur and
1292 chlorine in Late Cretaceous Deccan magmas and eruptive gas release. Science
1293 319, 1654-1657. doi: 10.1126/science.1152830
1294 Seyve, C., 1984. Le passage Crétacé-Tertiaire à Pont Labau. Bulletin des Centres de
1295 Recherches Exploration-Production Elf-Aquitaine, 8, 385–423.
1296
1297 Smit, J., and ten Kate, W.G.H.Z., 1982. Trace-element patterns at the Cretaceous–
1298 Tertiary boundary-consequences of a large impact Cretaceous Research, 3, 307–
1299 332.
1300
1301 Stüben, D., Kramar, U., Berner, Z. A., Meudt, M., Keller, G., Abramovich, S., Adatte, T.,
1302 Hambach, U. and Stinnesbeck, W. 2003. Late Maastrichtian paleoclimatic and
1303 paleoceanographic changes inferred from Sr/Ca ratio and stable isotopes.

1304 Palaeogeography, Palaeoclimatology, Palaeoecology, 199(1), 107-127. doi:
1305 10.1016/S0031-0182(03)00499-1
1306
1307 Subbarao, K.V., Bodas, M.S., Khadri, S.F.R., Beane, J.E., Penrose Deccan 2000, Field
1308 excursion guide to the western Deccan Basalt Province. Penrose Field Guides, B.
1309 Geological Society of India, ed., 2000.
1310
1311 Summesberger, H., Wagreich, M. and Bryda, G. 2009. Upper Maastrichtian cephalopods
1312 and the correlation to calcareous nannoplankton and planktic foraminifera zones
1313 in the Gams Basin (Gosau Group; Styria, Austria). Annalen des Naturhistorischen
1314 Museums Wien 111A, 159–182.
1315
1316 Tantawy, A. A., 2003. Calcareous nannofossil biostratigraphy and paleoecology of the
1317 Cretaceous-Tertiary transition in the central eastern desert of Egypt. Marine
1318 Micropaleontology, 47, 323-356. doi: 10.1016/S0377-8398(02)00135-4
1319
1320 Tantawy, A. A., Keller, G. and Pardo, A., 2009. Late Maastrichtian volcanism in the
1321 Indian Ocean: effects on calcareous nannofossils and planktic foraminifera.
1322 Palaeogeography, Palaeoclimatology, Palaeoecology, 284(1), 63-87.
1323 10.1016/j.palaeo.2009.08.025
1324
1325 Thibault, N. and Gardin, S., 2010. The calcareous nannofossil response to the end-
1326 Cretaceous warm event in the Tropical Pacific. Palaeogeography,

Palaeoclimatology, Palaeoecology, 291(3), 239-252. doi:10.1016/j.palaeo.2010.02.036

Thibault, N., Minoletti, F., Gardin, S., and Renard, M., 2004. Morphométrie de nannofossiles calcaires au passage Crétacé-Paléocène des coupes de Bidart (France) et d'Elles (Tunisie). Comparaison avec les isotopes stables du carbone et de l'oxygène. Bulletin de la Societe Géologique de France, 175.

Thunell, R. C., 1976. Optimum indices of calcium carbonate dissolution, in deep-sea sediments. Geology, 4(9), 525-528.

Vonhof, H.B. and Smit, J., 1997. High-resolution late Maastrichtian–early Danian oceanic $^{87}Sr/^{86}Sr$ record: implications for Cretaceous–Tertiary boundary events. Geology, 25, 347–350. doi: 10.1130/0091-7613(1997)025<0347:HRLMED> 2.3.CO;2

Wagreich, M., 1993. Subcrustal tectonic erosion in orogenic belts - A model for the Late Cretaceous subsidence of the Northern Calcareous Alps (Austria). Geology, 21, 941-944.

Wagreich, M., 1995. Subduction tectonic erosion and Late Cretaceous subsidence along the northern Austroalpine margin (Eastern Alps, Austria). Tectonophysics, 242, 63-78.

Wagreich, M. and Krenmayr, H., -G., 1993. Nannofossil biostratigraphy of the Late Cretaceous Nierental Formation, Northern Calcareous Alps (Bavaria, Austria). Zitteliana, 20, 67-77.

Wagreich, M. and Krenmayr, H., -G., 2005. Upper Cretaceous oceanic red beds (CORB) in the Northern Calcareous Alps (Nierental Formation, Austria): slope topography and clastic input as primary controlling factors. Cretaceous Research, 26, 57-64.

Widmark, J. G. V. and Malmgren, B. A., 1992. Benthic foraminiferal changes across the Cretaceous/Tertiary boundary in the deep sea; DSDP sites 525, 527, and 465. The Journal of Foraminiferal Research, 22(2), 81-113.

Williams, D. F., Healy-Williams, N. and Laschak, P., 1985. Dissolution and water-mass patterns in the southeast Indian Ocean, I, Evidence from Recent to late Holocene foraminiferal assemblages, Geological Society of America Bulletin, 96, 176–189.

Zeebe, R.E., 2012. History of seawater carbonate chemistry, atmospheric CO_2, and ocean acidification: Annual Review of Earth and Planetary Sciences, 40, 141–165, doi: 10.1146/annurev-earth-042711-105521.

Zeebe, R.E., Zachos, J.C., Caldeira, K., and Tyrrell, T., 2008. Carbon emissions and acidification. Science, 321, 51–52. doi:10.1126/science.1159124.

LIST OF FIGURES

Figure 1. Palaegeographic map of 66 Ma showing the study sections Bidart (France) and Gamsbach (Austria) and the reference section Elles (Tunisia, GSSP) relative to the location of the Reunion hotspot (focal point of Deccan volcanism). Modified after ©2000 C R Scotese PALEOMAP Project.

Figure 2. (A) Lithological log of the upper Maastrichtian-basal Danian interval studied at Bidart, the red layer marks the KTB (B) Google Earth image showing the present day location of Bidart (C) Field photograph of the Bidart section showing the sampled interval and the position of KTB (in red).

Figure 3. (A) Lithological log of the uppermost Maastrichtian interval of Gamsbach, the red layer marks the KTB (B) Google Earth image showing the present day location of Gamsbach (C) Field photograph of the Gamsbach section showing the position of KTB (in red).

Figure 4. The completeness of Bidart and Gamsbach sections relative to Elles (Tunisia) based on planktic foraminiferal biozonation scheme of Keller et al. (1995; 2002). The biozone ages can be extrapolated using a KTB age of 65.5 Ma (Gradstein et al., 2004) or 66.04 Ma (Renne et al., 2013). Hiatuses are observed at the KTB and at the P1a(1)/P1a(2) transition at Bidart. A major hiatus is identified at the KTB at Gamsbach due to missing zones P0, P1a(1) and early P1a(2).

Figure 5. (A) Key foraminifera and geochemical attributes of the KTB boundary and lower Danian at Bidart (B) Abundance of late Maastrichtian planktic foraminifera of the 63-150 μm size fraction and the KTB mass extinction. The $\delta^{13}C$ record shows the characteristic ~2‰ negative shift at the KTB.

Figure 6. (A) Faunal and geochemical changes at the KTB boundary and in the lower Danian of Gamsbach. (B) Late Maastrichtian planktic foraminifera of the >150 μm size fraction and the KTB mass extinction. The $\delta^{13}C$ record shows ~1.3‰ negative shift at the KTB.

Figure 7. A comparison of the relative abundances of some key species (63-150 μm) in the upper Maastrichtian zone CF1 assemblage of (A) Elles (Tunisia) and (B) Bidart (France). Note that *Heterohelix dentata*, *H. globulosa* and *Pseudoguembelina costulata* dominate the assemblage in Elles, in contrast to Bidart where they are rare. Whole-rock $\delta^{13}C$ and $\delta^{18}O$ are shown.

Figure 8. A comparison of the relative abundances of some key species (>150 μm) in the Late Maastrichtian zone CF1 assemblage of (A) Elles (Tunisia), (B) Bidart (France) and (C) Gamsbach (Austria). The deep-water assemblages of Bidart and Gamsbach are very similar to each other and different from the neritic assemblages of Elles. Planktic $\delta^{13}C$ and $\delta^{18}O$ for Elles are obtained from *Rugoglobigerina rugosa* and benthic values are

1418 from *Cibicidoides pseudoacuta.* Whole-rock isotope data are shown for the Bidart and
1419 Gamsbach sections.
1420
1421 **Figure 9**. Relative abundances of depth-ranked groups of planktic foraminifera species in
1422 (A) Elles (Tunisia), (B) Bidart (France) and (C) Gamsbach (Austria). Thermocline
1423 dwelling globotruncanids (blue) are more abundant in the >150 μm fraction of Bidart and
1424 Gamsbach (open marine settings) as compared to Elles (neritic setting). Poor preservation
1425 of foraminifera in the 63-150 μm fraction of the Gamsbach section precluded quantitative
1426 analysis.
1427
1428 **Figure 10**. Multi-proxy data shows a dissolution interval immediately preceding the
1429 KTB. A low magnetic susceptibility (MS) interval in the upper part of zone CF1 of Elles,
1430 Bidart and Gamsbach (yellow) marks a regional chemical benchmark of Deccan
1431 volcanism (after Font et al, 2011; 2014). Increased planktic foraminiferal test
1432 fragmentation in the low MS interval supports water column carbonate dissolution.
1433
1434 Figure 11. Magnetic susceptibility (MS) data for Bidart (Font et al., 2011) along with the
1435 fragmentation index (FI) data for planktic and benthic foraminifera. The geochemical
1436 Deccan benchmark interval coincides with a pronounced water column dissolution event
1437 recorded by the planktic foraminifera. The benthic FI for the same interval indicate only a
1438 minor contribution of post-depositional breakage.
1439
1440

Plate 1. Characteristic taxa of the upper Maastrichtian zone CF1 assemblage at Bidart, France, scale bar= 100 μm.

A. *Globotruncanita stuarti* (de Lapparent), spiral view

B. *Abathomphalus mayaroensis* (Brönnimann), spiral view

C. *Heterohelix rajagopalani* Govindan

D. *Pseudoguembelina hariaensis* Nederbragt

E. *Heterohelix globulosa* (Ehrenberg)

F. *Pseudotextularia elegans* (Rzehak)

G. *Racemiguembelina fructicosa* (Egger)

H. *Planoglobulina brazoensis* (Martin)

I. *Guembelitria cretacea* (Cushman)

J. *Spiroplecta americana* (Ehrenberg)

K. *Hartella harti* Georgescu & Abramovich

L. *Heterohelix navarroensis* (Loeblich)

M. *Plummerita* aff. *hantkeninoides* (Brönnimann)

N. *Rugoglobigerina macrocephala* (Brönnimann)

O. *Globigerinelloides volutus* (White)

P. *Globigerinelloides subcarinatus* (Brönnimann)

Plate 2. Planktic foraminifera indicating varying degrees of preservation in the upper Maastrichtian zone CF1 assemblage at Bidart, France, scale bar= 100 μm.

(A-L): “Imperfect” tests with minor breakages and/or holes and signs test surface dissolution

(M-S): “Fragments” defined by less than two-thirds or the original test preserved.

Plate 3. Benthic foraminifera indicating varying degrees of preservation in the upper Maastrichtian zone CF1 and the KTB assemblage at Bidart, France, scale bar= 100 μm.

(A-G): “Perfect” tests with no signs of chemical or mechanical damage

(H-L, O, P): “Imperfect” tests with minor breakages and/or holes and signs test surface dissolution. Note that the proportion of the tests with holes is maximum at the KTB and in the early Danian sediments.

(M, N, Q-S): “Fragments” defined by less than two-thirds or the original test preserved.

Figure1. Paleogeographic Map

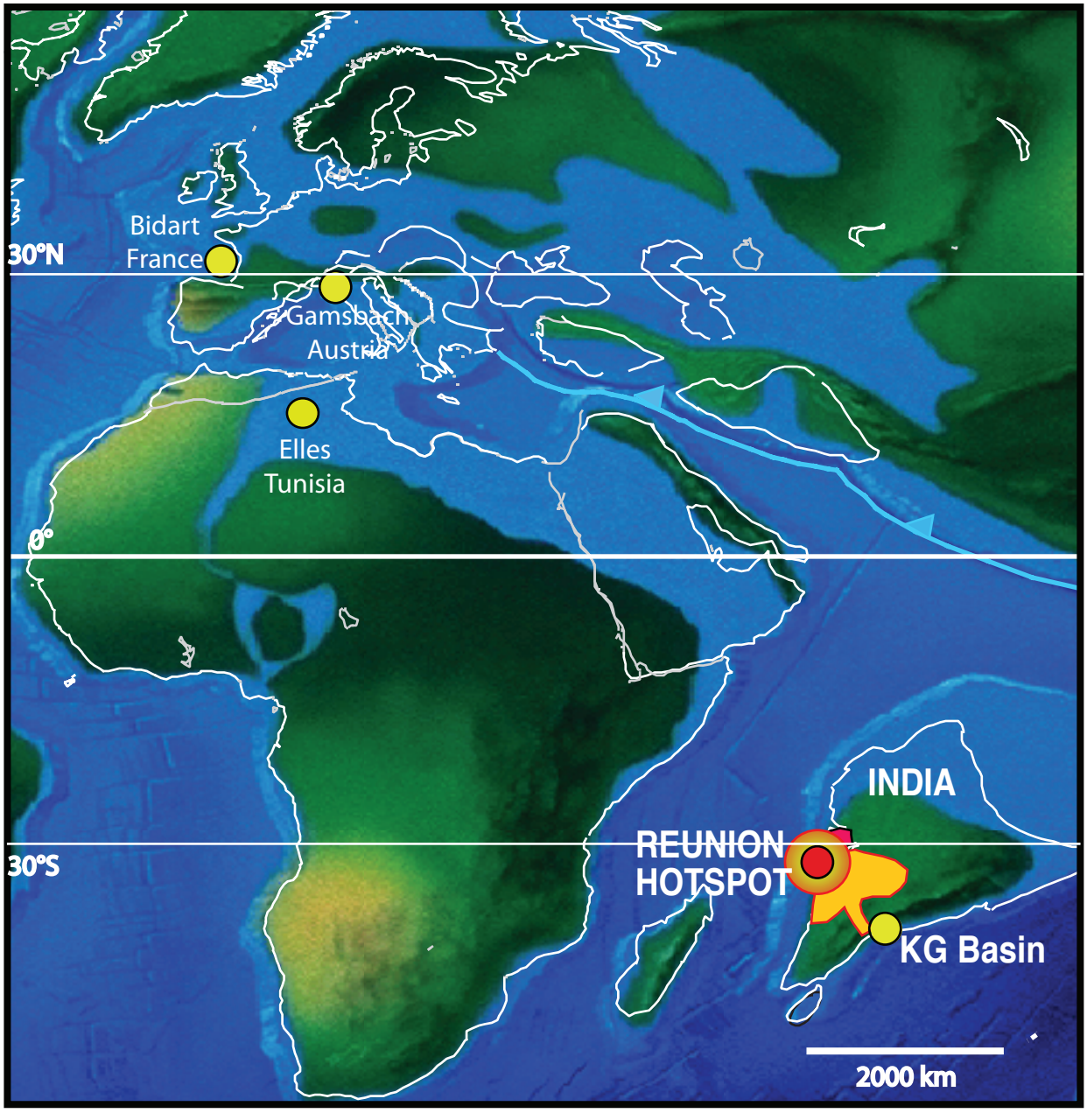

Figure2. Location_Lithology_Bidart

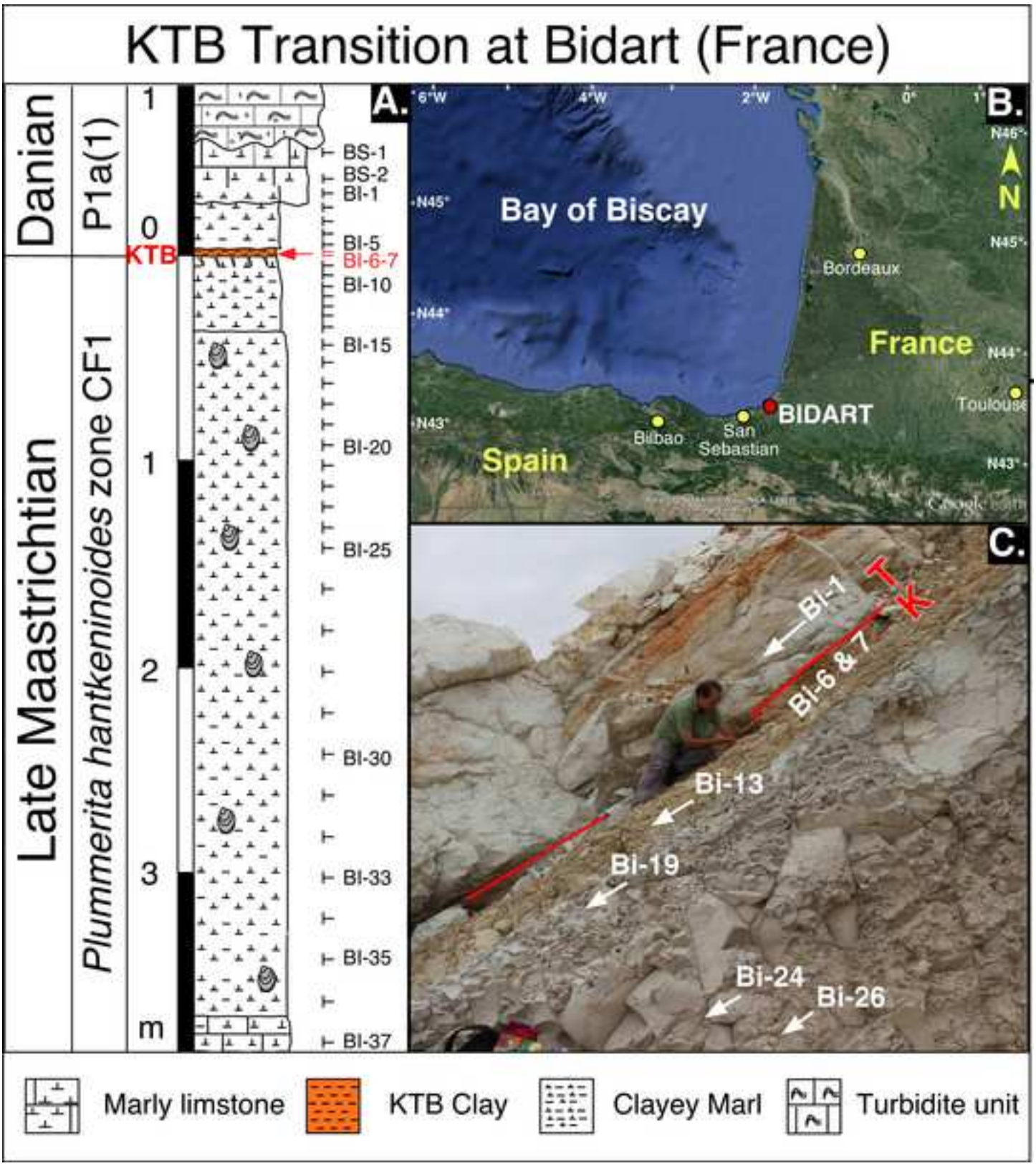

Figure3. Location_Lithology_Gamsabch

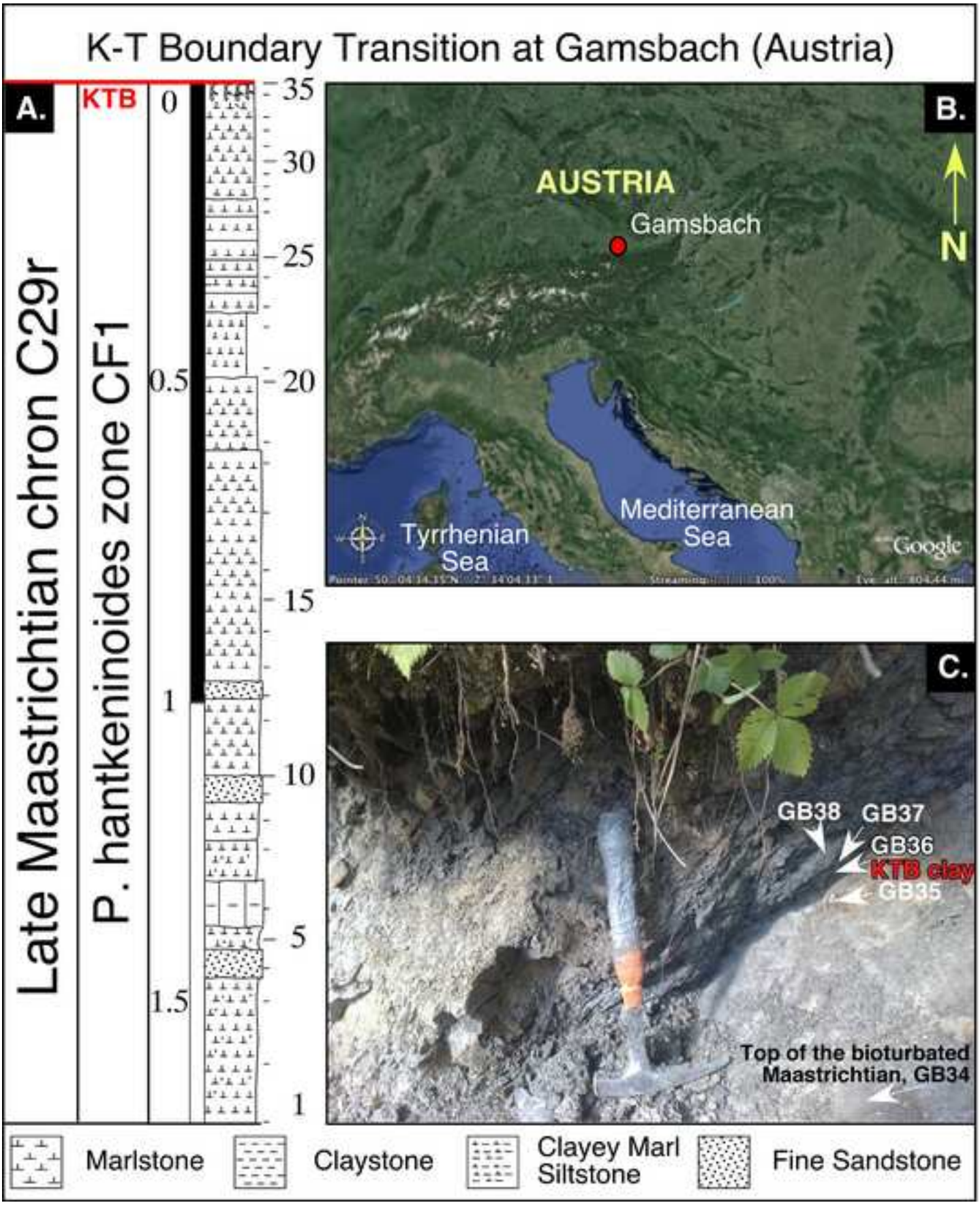

Figure4. Biostratigraphic zones

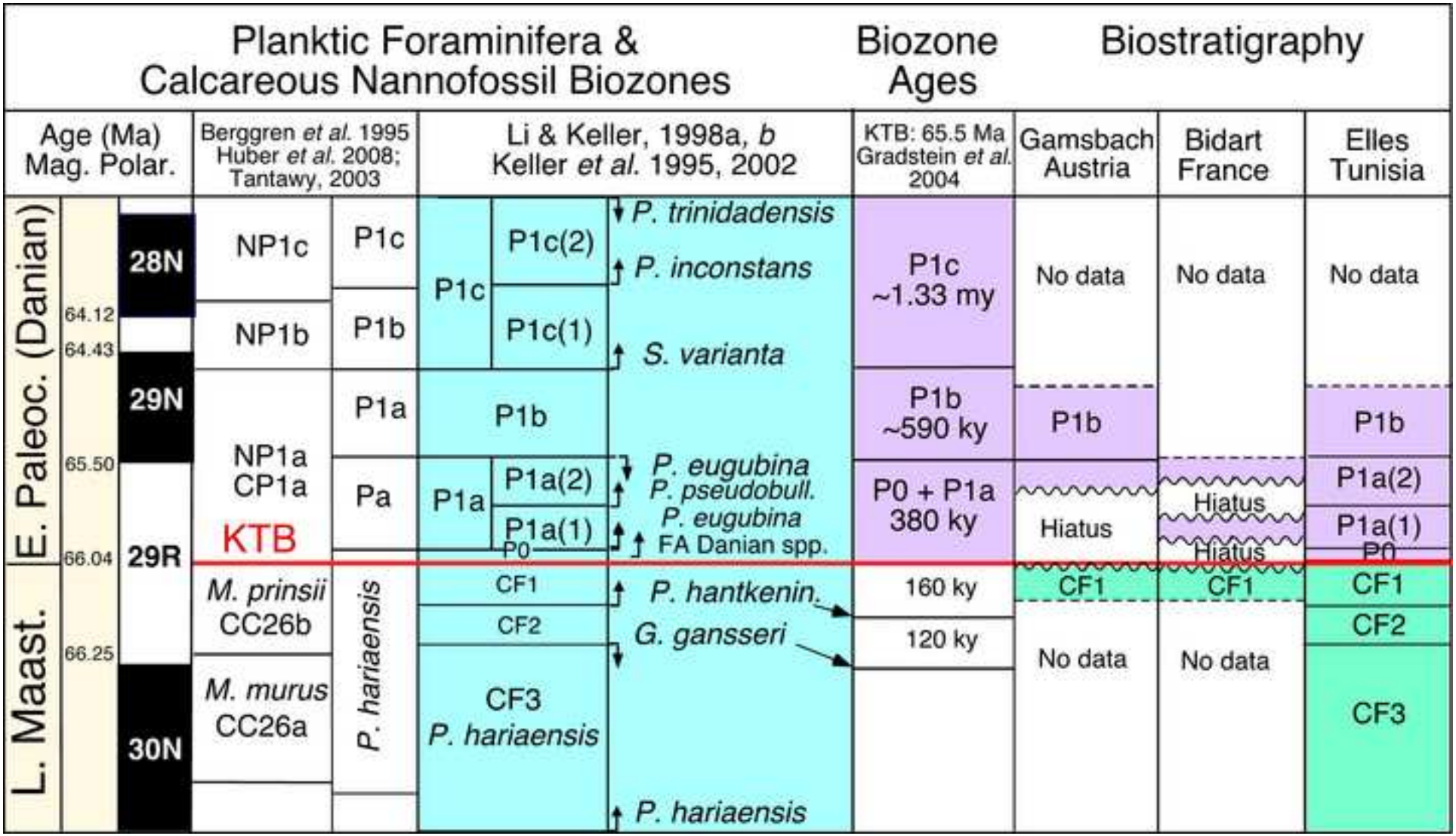

Figure5A. Bidart Early Danian

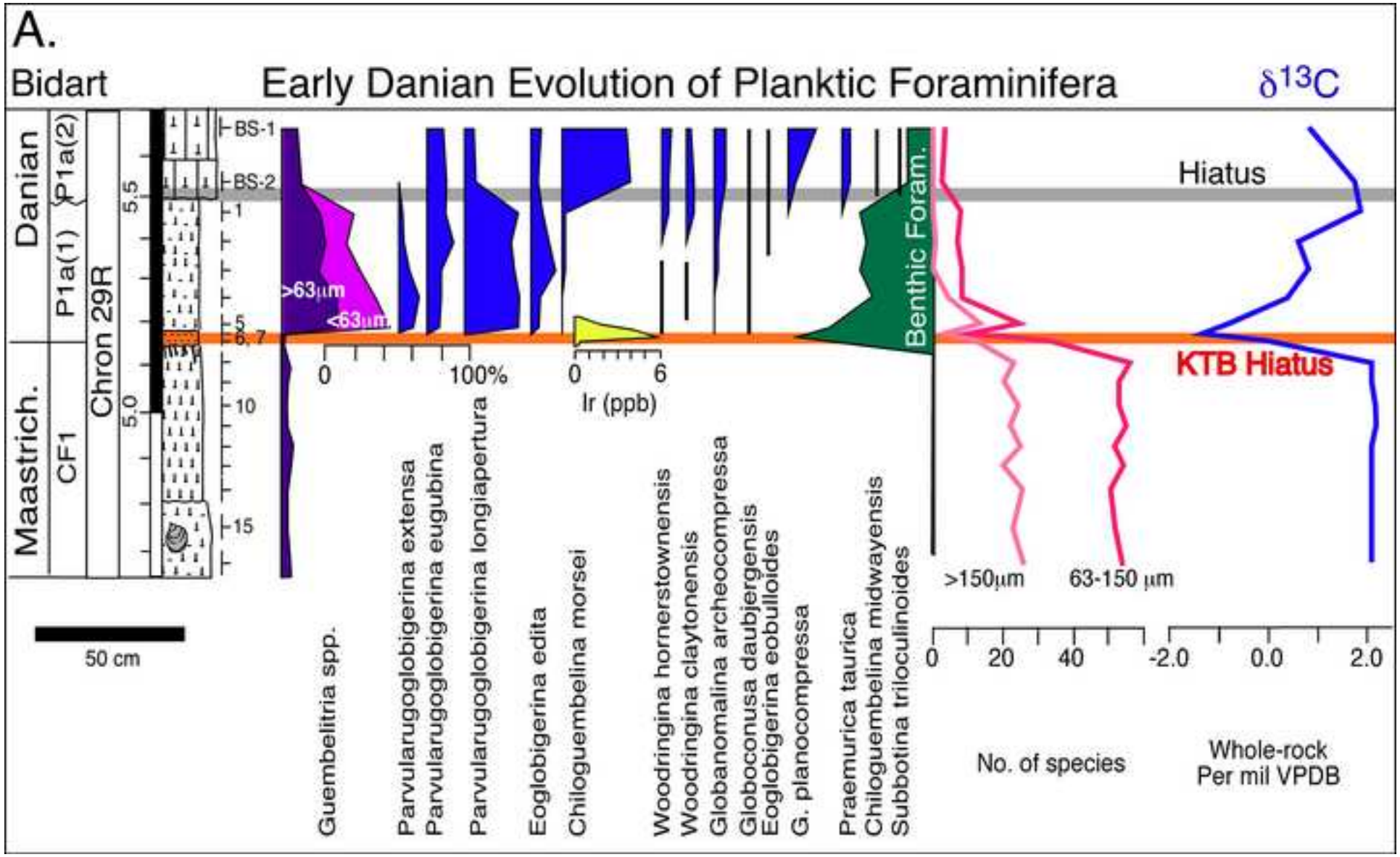

Figure5B. Bidart Late Maastrichtian (63-150um)

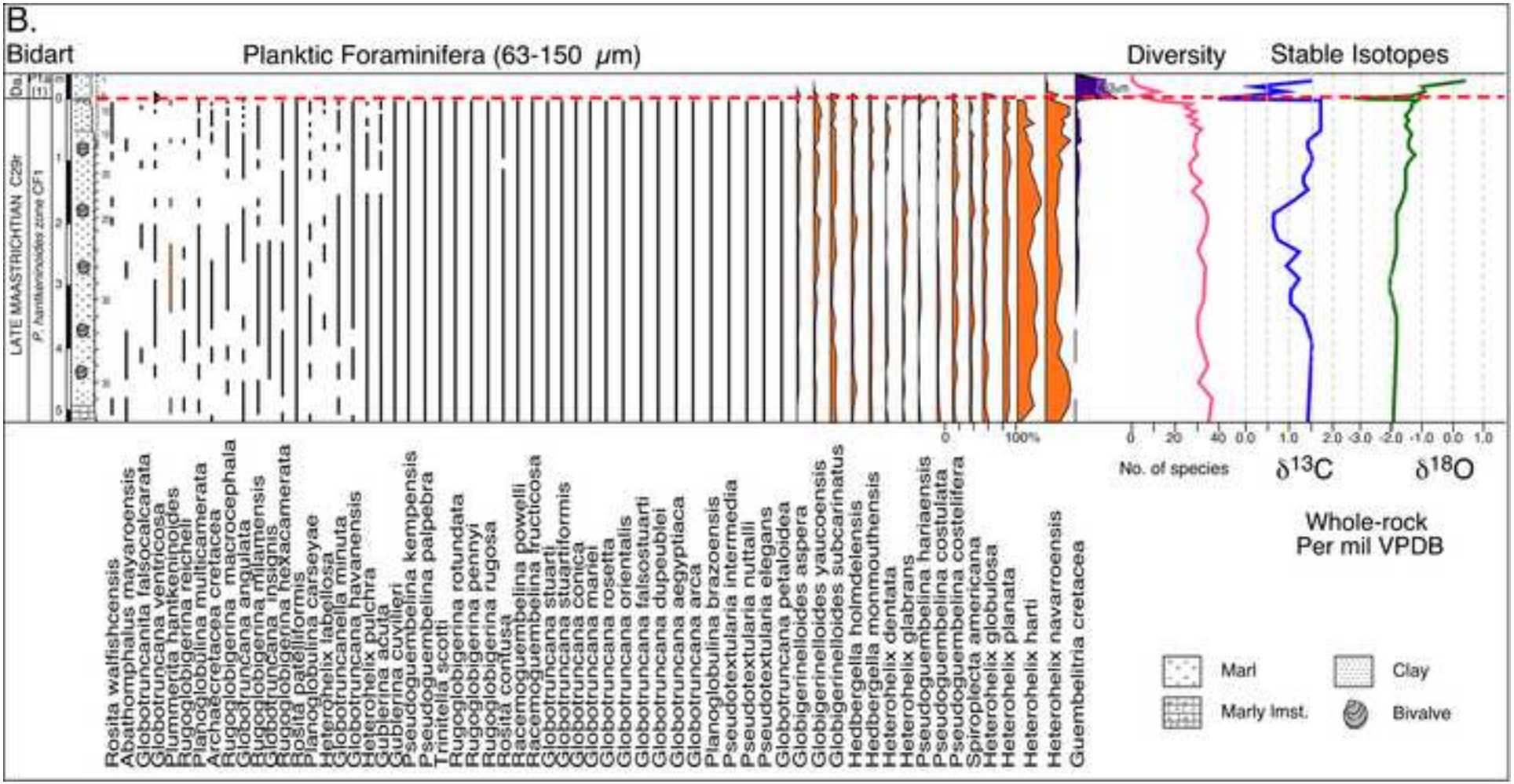

Figure6A. Gamsbach Early Danian

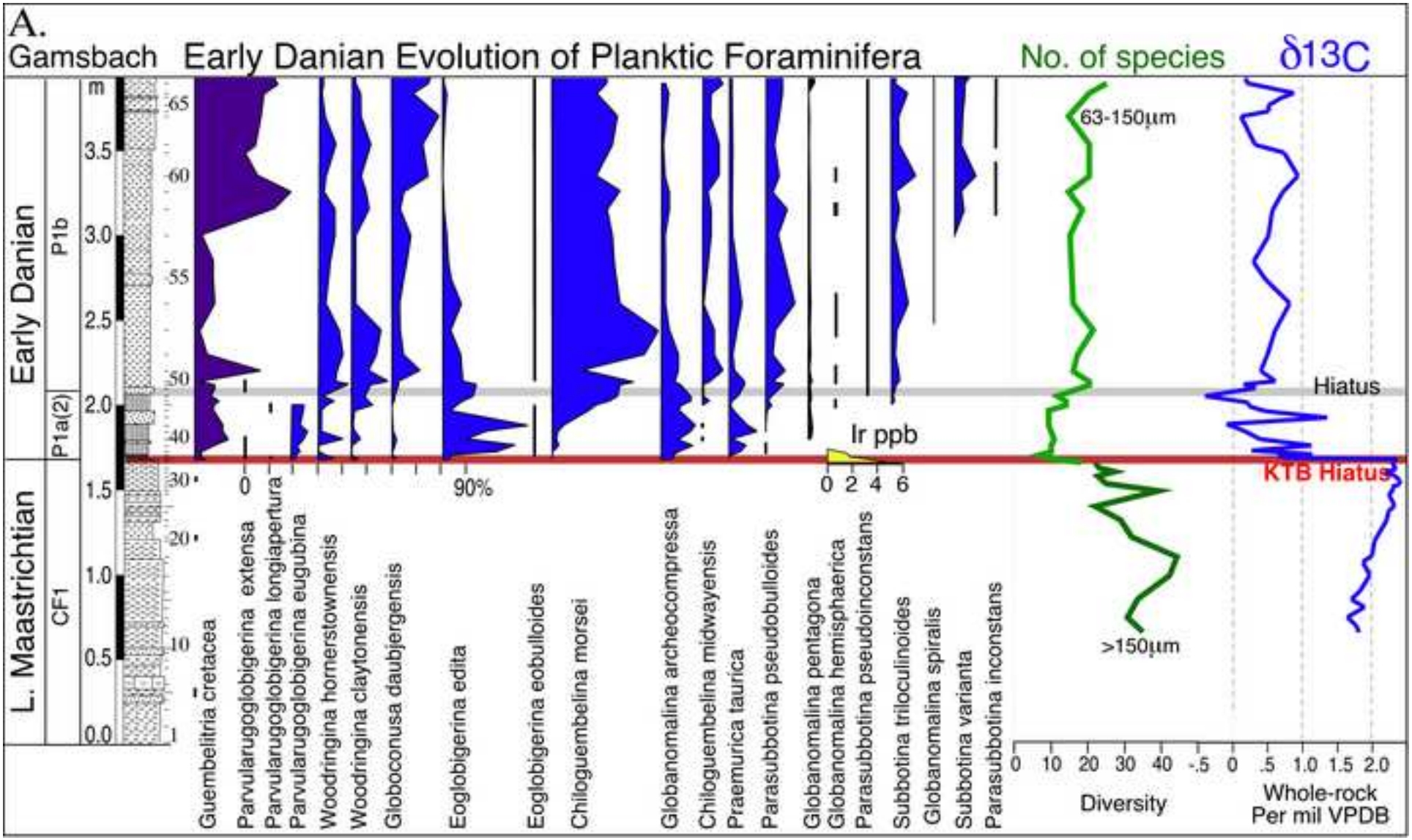

Figure6B. Gamsbach Late Maastrichtian (>150um)

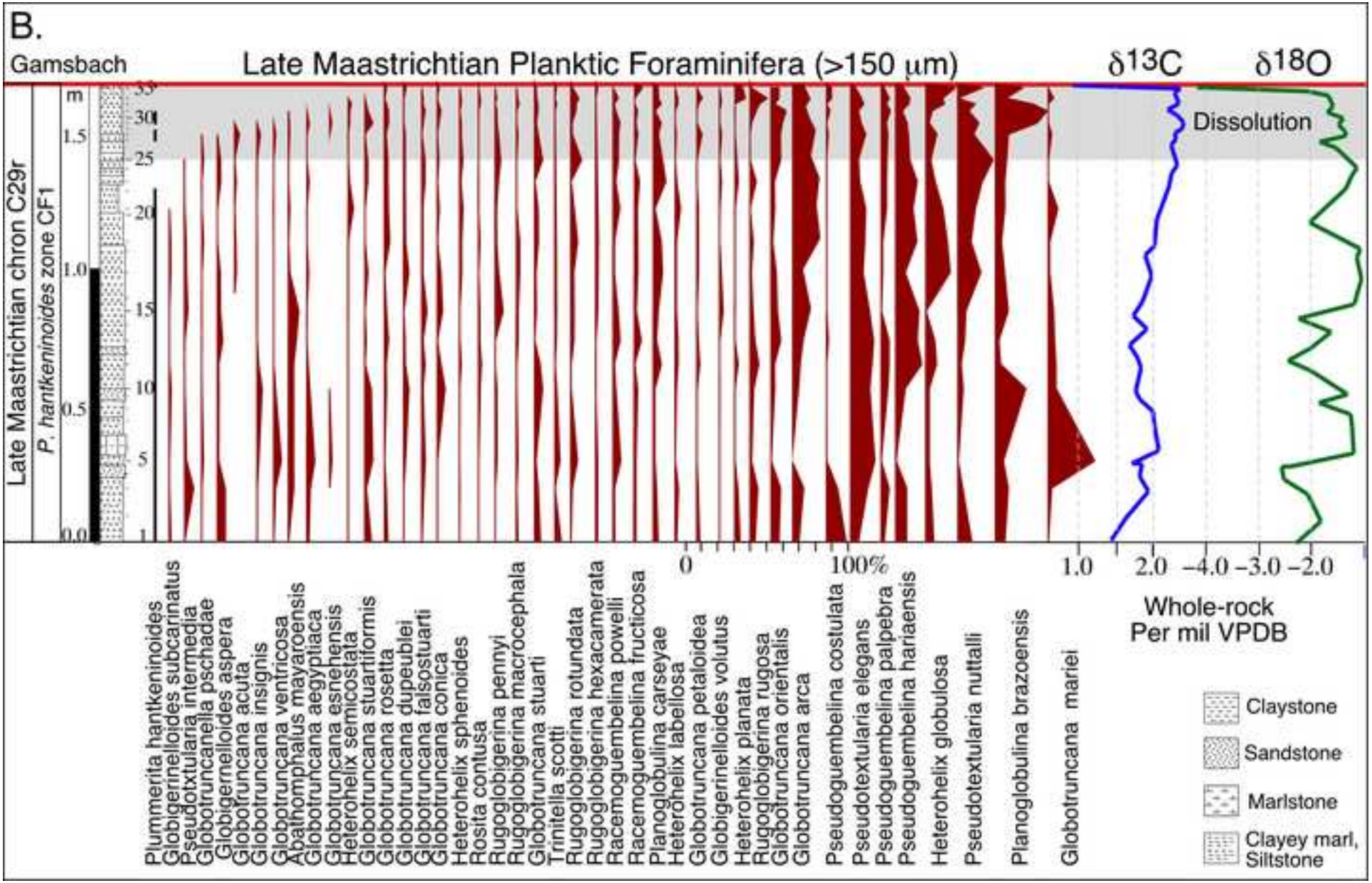

Figure7.AB. Key Species (63-150um) and stable isotopes

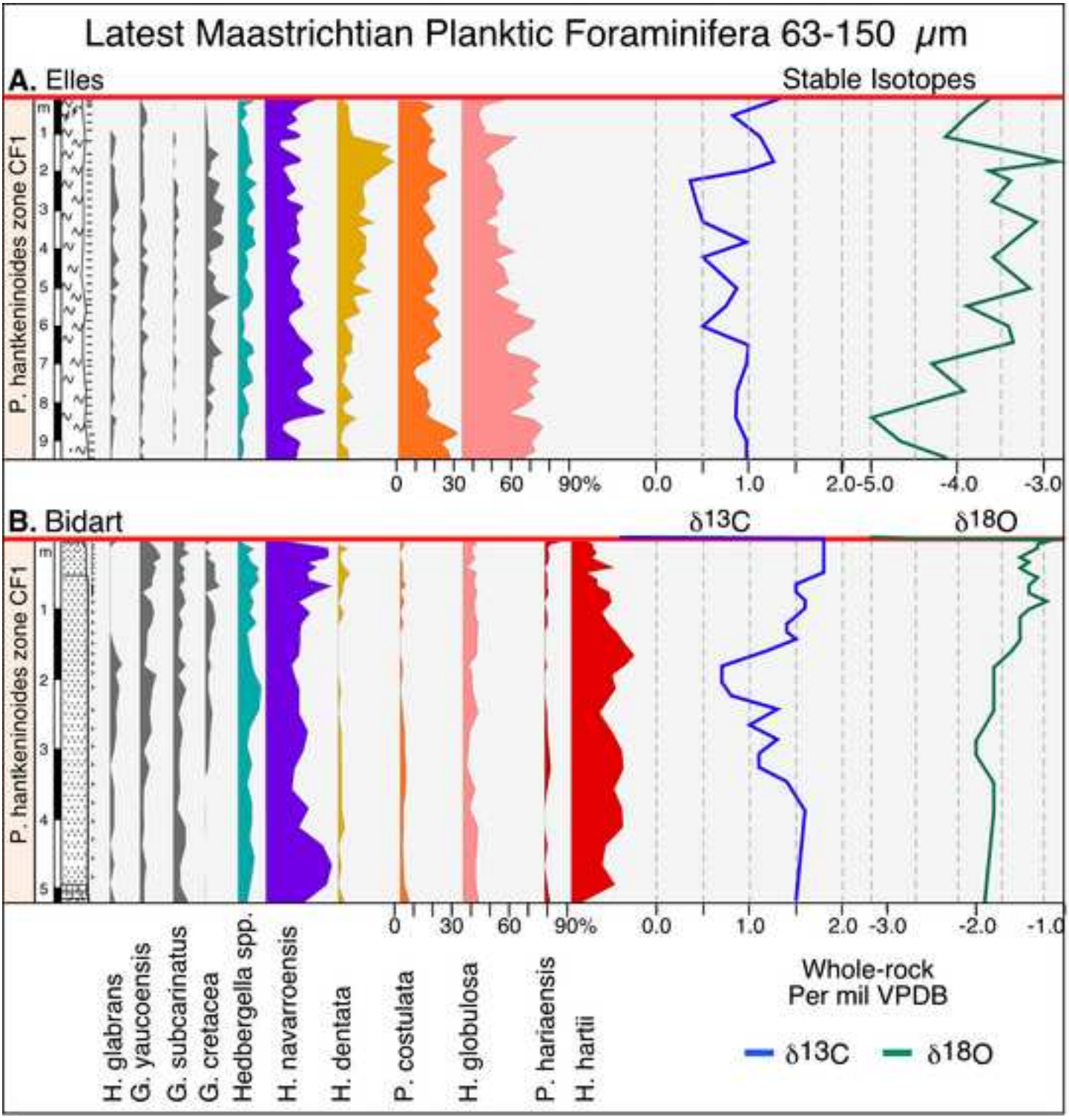

Figure8.ABC. Key Species (>150um) and stable isotopes

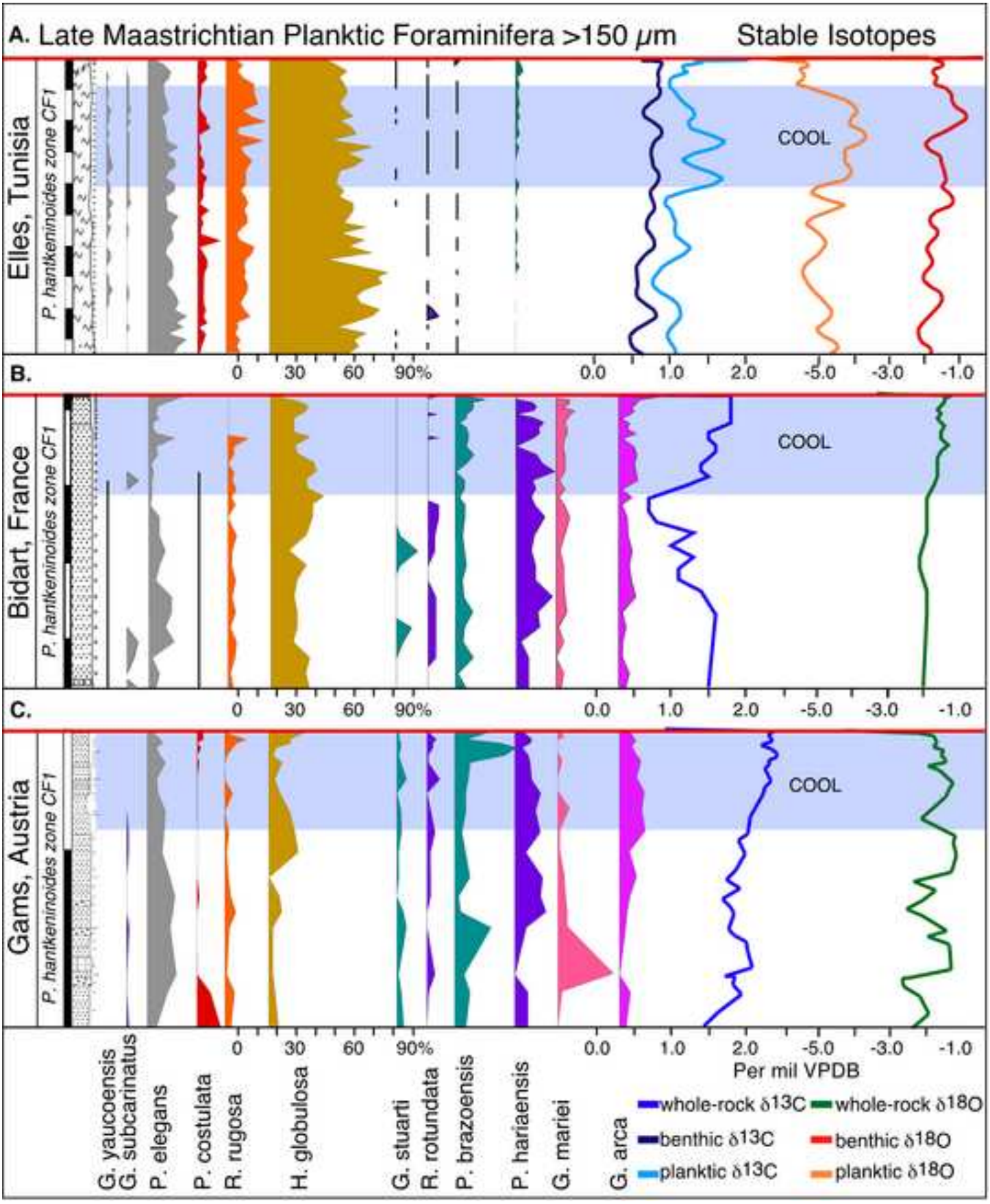

Figure9.ABC. Depth ranked Species

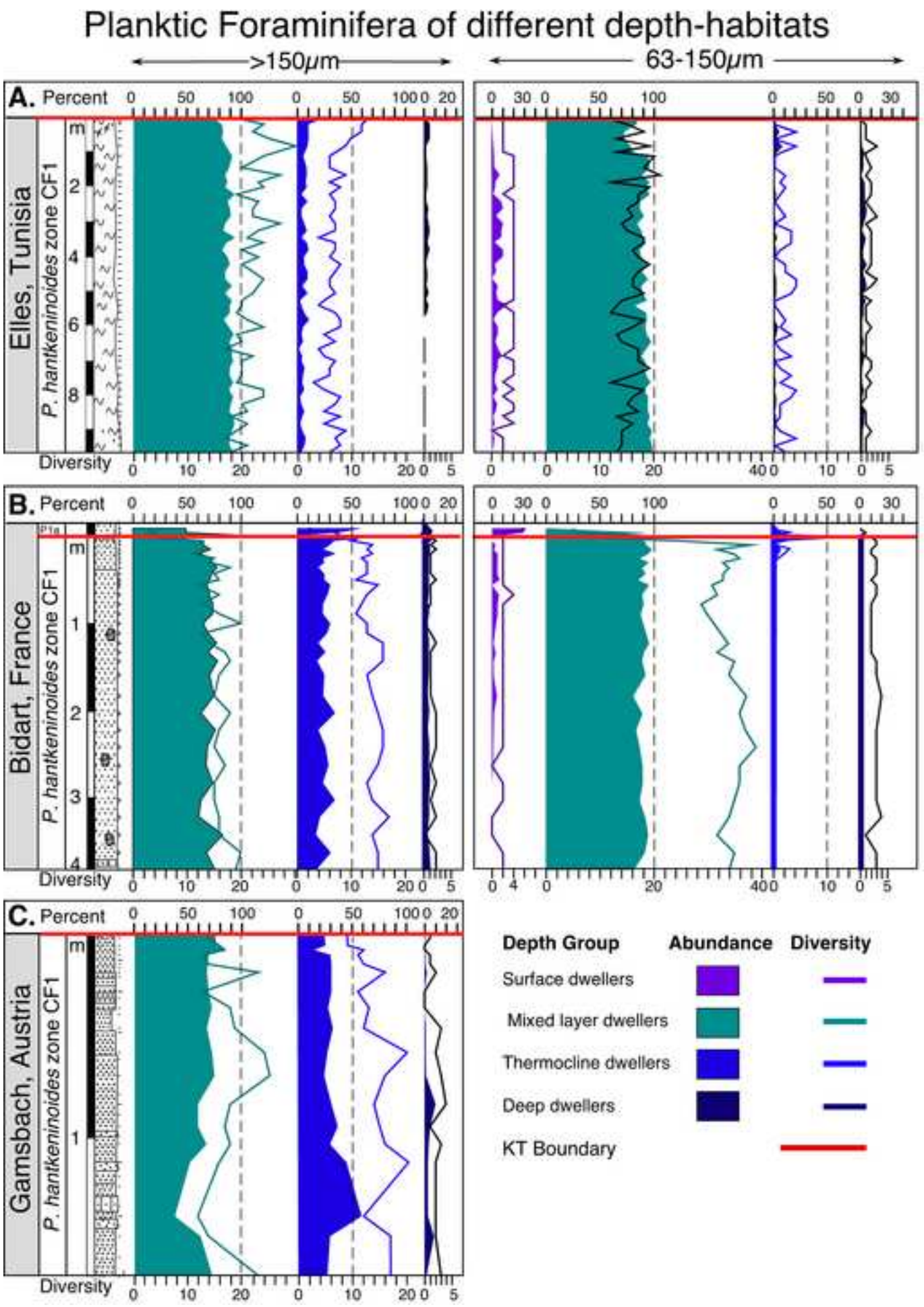

Figure10.ABC. Multi-proxy evidence for ocean acidification

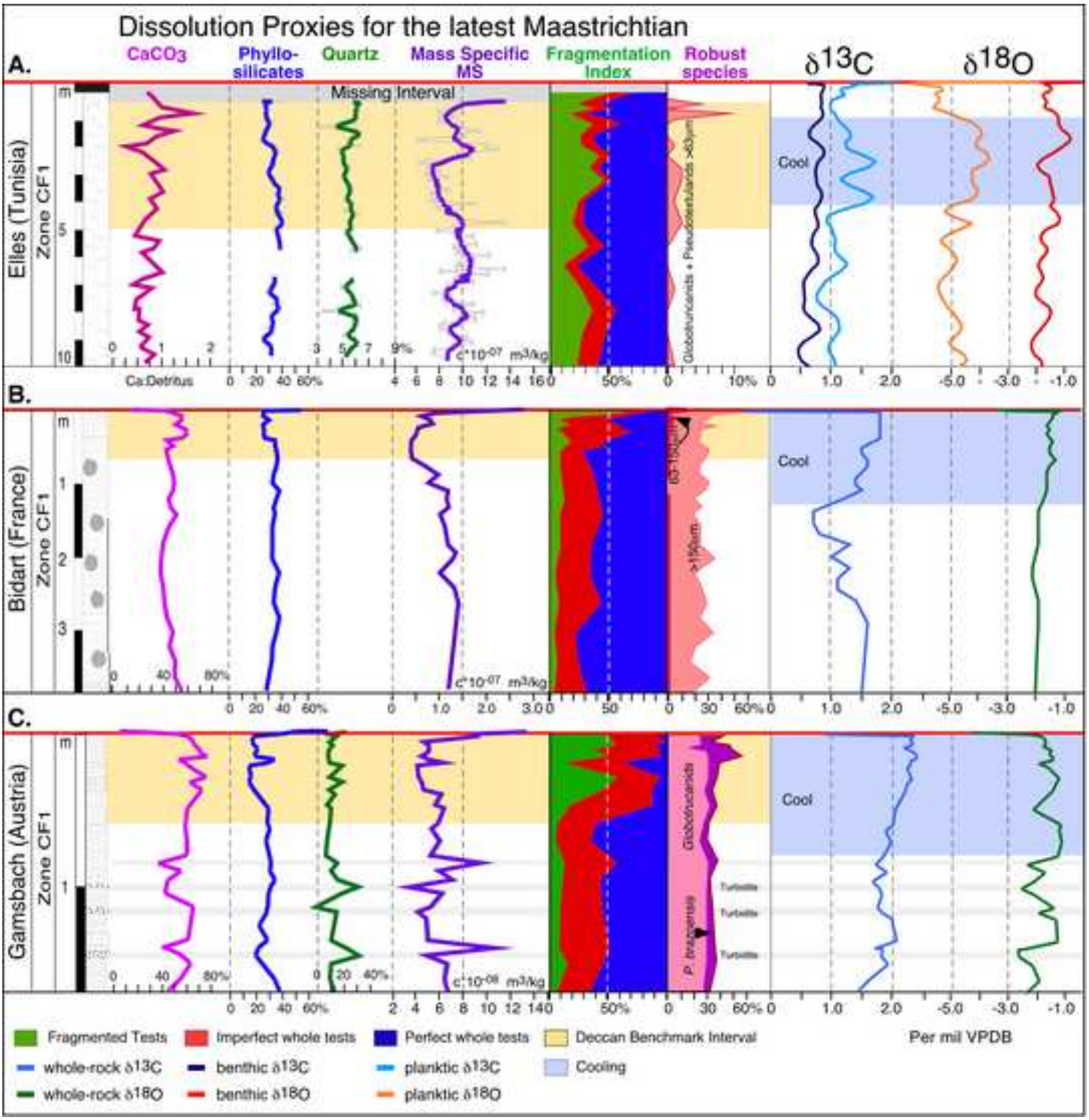

Figure11. Planktic vs. Benthic Fragmentation Index

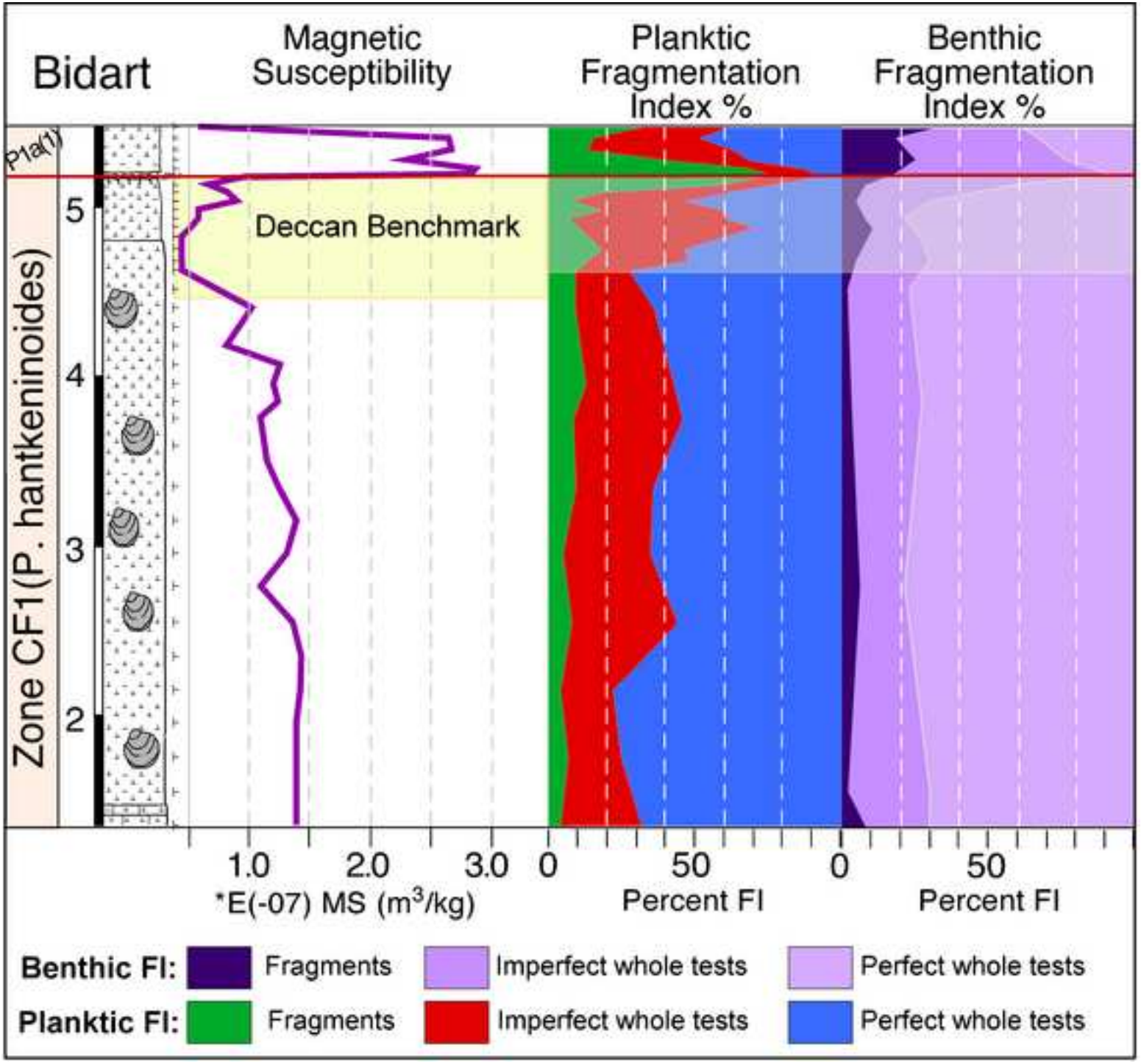

Plate1. Bidart Planktic Foraminifera

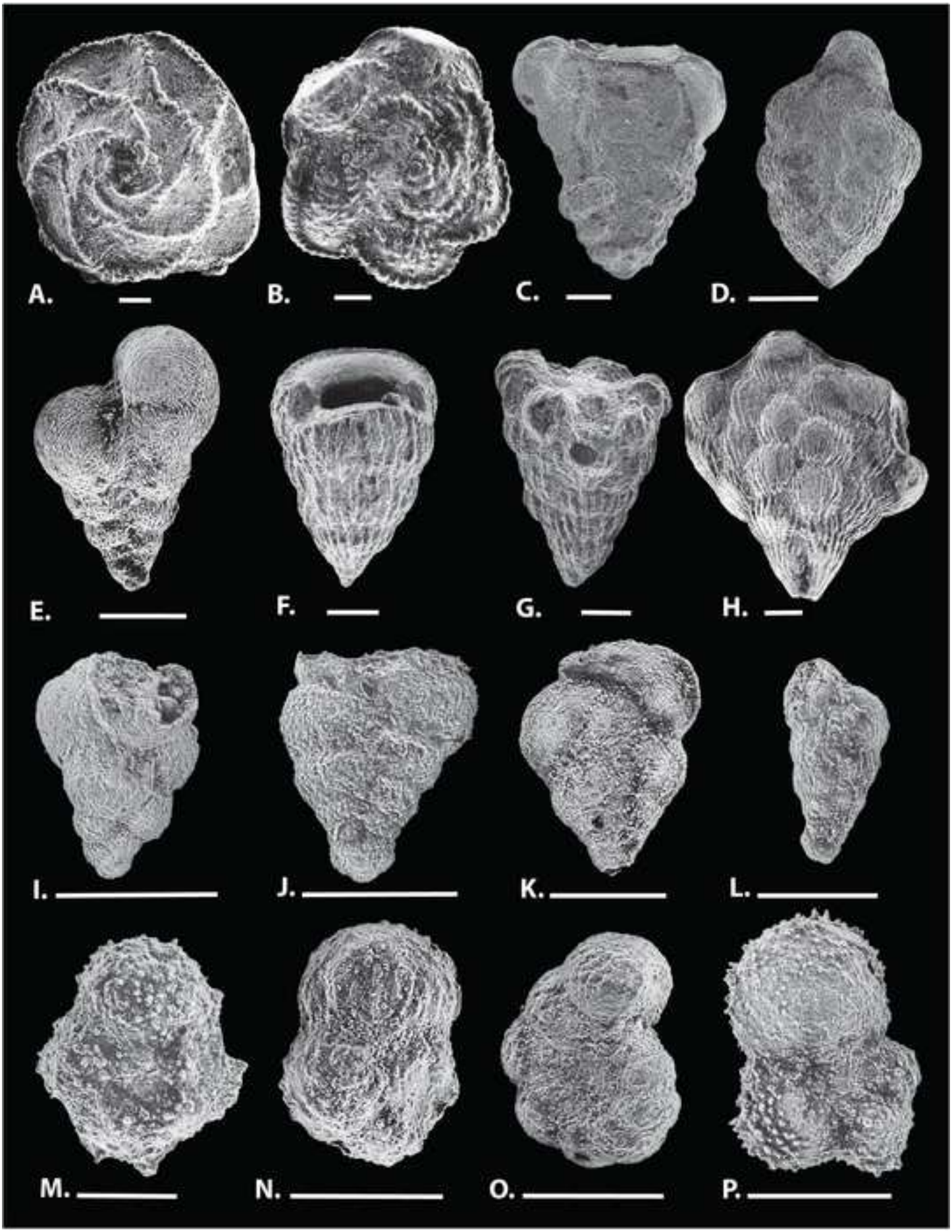

Plate2. Planktic Foraminifera Preservation

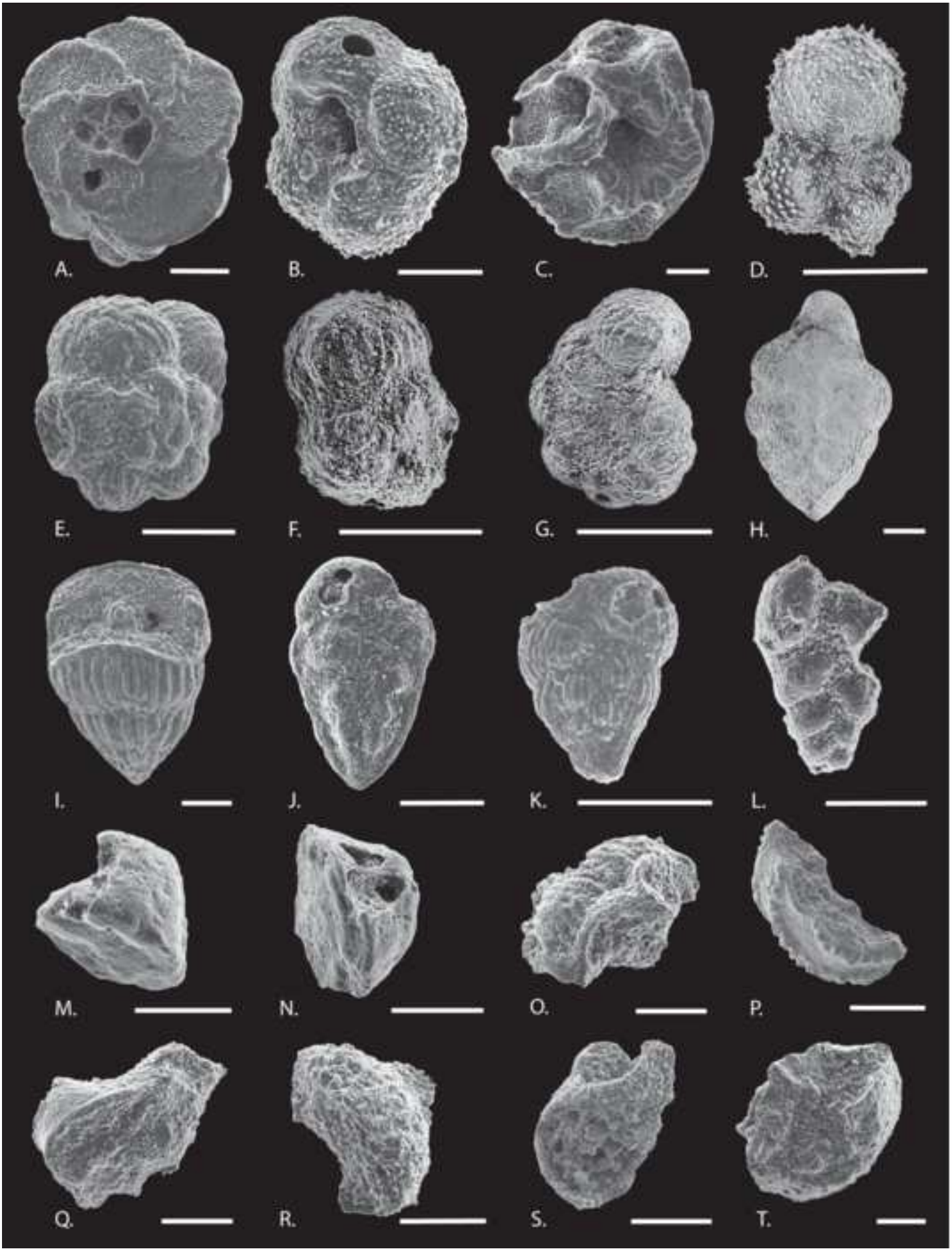

Plate3. Benthic Foraminifera Preservation